Summer 2021

Early wildfire detection by air quality sensors on unmanned aerial vehicles: Optimization and feasibility

Doaa Rjoub

Department:

EARLY WILDFIRE DETECTION BY AIR QUALITY SENSORS ON UNMANNED AERIAL VEHICLES: OPTIMIZATION AND FEASIBILITY

by

DOAA RJOUB

A THESIS

Presented to the Graduate Faculty of the

MISSOURI UNIVERSITY OF SCIENCE AND TECHNOLOGY

In Partial Fulfillment of the Requirements for the Degree

MASTER OF SCIENCE

in

CIVIL ENGINEERING

2021

Approved by:

Yang Wang, Advisor
Guang Xu
Maciej Zawodniok

ABSTRACT

Millions of acres of forests are destroyed by wildfires every year, causing ecological, environmental, and economical losses. The recent wildfires in Australia and the Western U.S. smothered multiple states with more than fifty million acres charred by the blazes. The warmer and drier climate makes scientists expect increases in the severity and frequency of wildfires and the associated risks in the future. These inescapable crises highlight the urgent need for early detection and prevention of wildfires. This work proposed an energy management framework that integrated unmanned aerial vehicle (UAV) with air quality sensors for early wildfire detection and forest monitoring. An autonomous patrol solution that effectively detects wildfire events, while preserving the UAV battery for a larger area of coverage was developed. The UAV can send real-time data (e.g., sensor readings, thermal pictures, videos, etc) to nearby communications base stations (BSs) when a wildfire is detected. An optimization problem that minimized the total UAV's consumed energy and satisfied a certain quality-of-service (QoS) data rate were formulated and solved. More specifically, this study optimized the flight track of a UAV and the transmit power between the UAV and BSs. Finally, selected simulation results that illustrate the advantages of the proposed model were proposed.

ACKNOWLEDGMENTS

In the name of Allah, the most merciful, the most beneficent, all praise and thanks for Allah, the Lord of the universe, for helping me to complete this work. I would like to take this opportunity to express my thanks to those who helped me with various aspects of conducting research and writing this work. First and foremost, I thank my supervisor Dr. Yang Wang for his support and guidance in almost every step to complete my work. I also thank my committee members Dr. Guang Xu and Dr. Maciej Zawodniok for their constructive comments and suggestions for this work.

TABLE OF CONTENTS

LIST OF ILLUSTRATIONS

LIST OF TABLES

NOMENCLATURE

Symbol	Description
B_0	Communication bandwidth
$C(x, y, z)$	Steady-state concentration at a point(x,y,z).
E_C	Total UAV communications energy.
E_F	Total UAV flying energy.
E_{tot}	Total UAV energy.
G	Earth gravity.
H	Effective height of the emission point.
K_a	Ambient air temperature.
K_s	Temperature of the plume.
N_0	Noise power
$PL_l^{\text{LoS}}[t]$	Line-of-sight path loss between the UAV and BS l during time t.
$PL_l^{\text{NLoS}}[t]$	Non-line-of-sight path loss between the UAV and BS l during time t.
$P_C[t]$	Total transmitted power during time t.
$P_F[t]$	Flying power at time t.
P_a	Ambient pressure.
$P_n[t]$	UAV's transmit power allocated for data type n.
P_s	Consumed power due to UAV hardware.

Q	Emission rate.
$R_{th,n}$	Data rate threshold of type n.
V	UAV speed.
Δx	Horizontal spacing distance or horizontal gap.
$\Theta_l[t]$	elevation angle between the UAV and BS l in degree.
$\bar{P}$	UAV transmit power budget.
$\bar{x}$	Maximum horizontal spacing distance.
δ	Number of quantization levels.
$\epsilon_l[t]$	Association between the UAV and BS l during time t.
$\hat{T}$	Time slot duration.
$\hat{U}[t]$	UAV location during time t.
κ	Emission rate factor.
ν_s	Upward velocity of the plume
ω_p	Number of the UAV propellers.
ψ	Air density
$\rho[t]$	Wildfire binary variable indication at time t.
$\sigma[t]$	Data rate loss-factor.
$\sigma_y(x)$	Horizontal spread parameters.
$\sigma_z(x)$	Vertical spread parameters.
τ	Genetic algorithm survival strings.

θ_w	Wind direction.
ξ_{LoS}	Line-of-sight shadowing loss.
ξ_{NLoS}	Non-line-of-sight shadowing loss.
d_s	Diameter of the plume at the emission point.
$g_l[t]$	Average channel gain between the UAV and BS l during time t.
h_0	Height of the plume on fire.
m_{tot}	UAV mass.
r_p	Radius of the UAV.
u	Average wind speed
z	Vertical distance from the plume centerline.

1. INTRODUCTION

Wildfires destroy millions of acres of forests every year, causing ecological, environmental, and economic damages. During the last decade, the severity and number of wildfires increased dramatically worldwide [1]. In 2018, approximately 8.7 million acres burned in the United States (U.S.) only, which cost around 24 billion dollars due to infrastructure damage and firefighting. The recent wildfires in Australia and Western U.S. smothered multiple states with more than fifty million acres charred [1]. Due to climate change, the severity and frequency of the wildfire and the risks associated with it are expected to increase in the future [2]. Given the fast speed of wildfire development, early detection is a key solution to ensure that fires are kept under control and properly extinguished. Figure 1.1 shows images of a recent wildfire in Saddleridge, California, near Los Angeles in 2019 [3]. This wildfire resulted in deaths of two people and the evacuation of approximately 100,000 people.

1.1. CURRENT DETECTION TECHNIQUES

Watchtowers. A conventional method for wildfire detection utilizes lookout stations situated with extensive visibility [4]. Figure 1.2-a and Figure 1.2-b show fire lookout towers in southern Georgia, U.S. and in Poland [5]. This method consumes tremendous labor costs and is subject to issues with workers' safety in fire detection [6, 7]. Furthermore, this method may delay fire detection (i.e, the worker maybe late in observing or reporting the fire event).

Satellite Remote Sensing. Satellite remote sensing is one of the most effective ways for monitoring forest fire activities [8]; they can identify active fires, evaluate burned areas, and assess fire emissions [9, 10]. Figure 1.3 shows satellite images provided by National Aeronautics and Space Administration (NASA) that detected a 2019 wildfire in

California [11]. However, satellite imagery has limited spatial resolution (tens of meters) and requires the observed area to be cloud-free, thus making it difficult to identify early-stage wildfires [12].

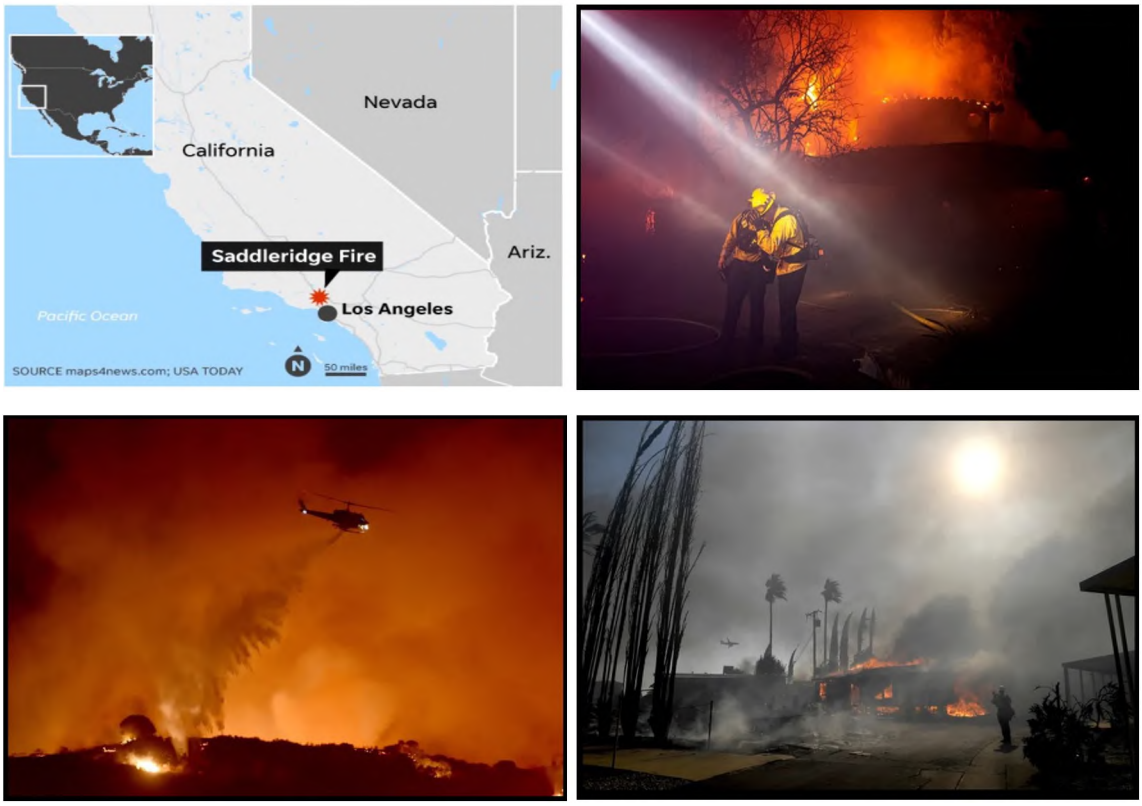

Figure 1.1. Pictures from Saddleridge fire erupts in California in 2019.

Thermal Imaging. Thermal imaging detects and monitors fire. This method can be utilized for detecting hotspots during fire mapping and tracking fire progression. Figure 1.4 shows a thermal image provided by the United States Geological Survey (USGS) taken in Florida in 2000 [13]. Several projects in the U.S. and worldwide aim to deploy large numbers of thermal cameras in hotspot locations and in forests. For example, as shown in Figure 1.5, a project taking place in California, U.S., called ALERTWildfire project, has installed 300 fixed thermal cameras in California forests with the goal of installing approximately 1,000

stations with advanced camera by 2022 [14]. However, thermal cameras are subject to limited spatial resolution and weather interference. Thick canopies may block the thermal signal from the fire [15].

Figure 1.2. Existing watchtowers, a) Fire lookout tower in South Georgia, United States, b) Fire lookout tower in Poland.

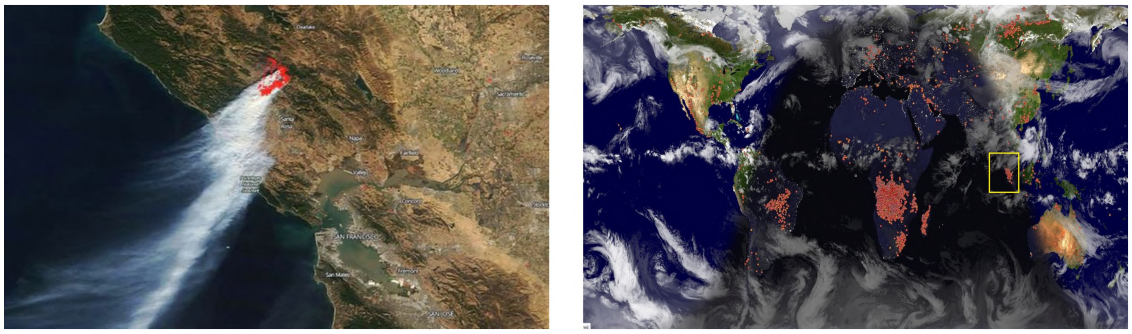

Figure 1.3. NASA satellite images in 2019, California United States.

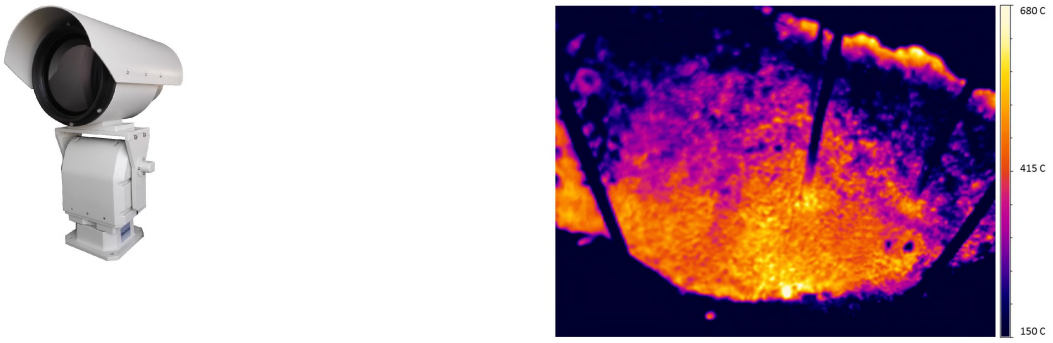

(a) (b)

Figure 1.4. Thermal imaging, a) Fixed thermal camera, b) A thermal image provided by USGS taken in Florida in 2000.

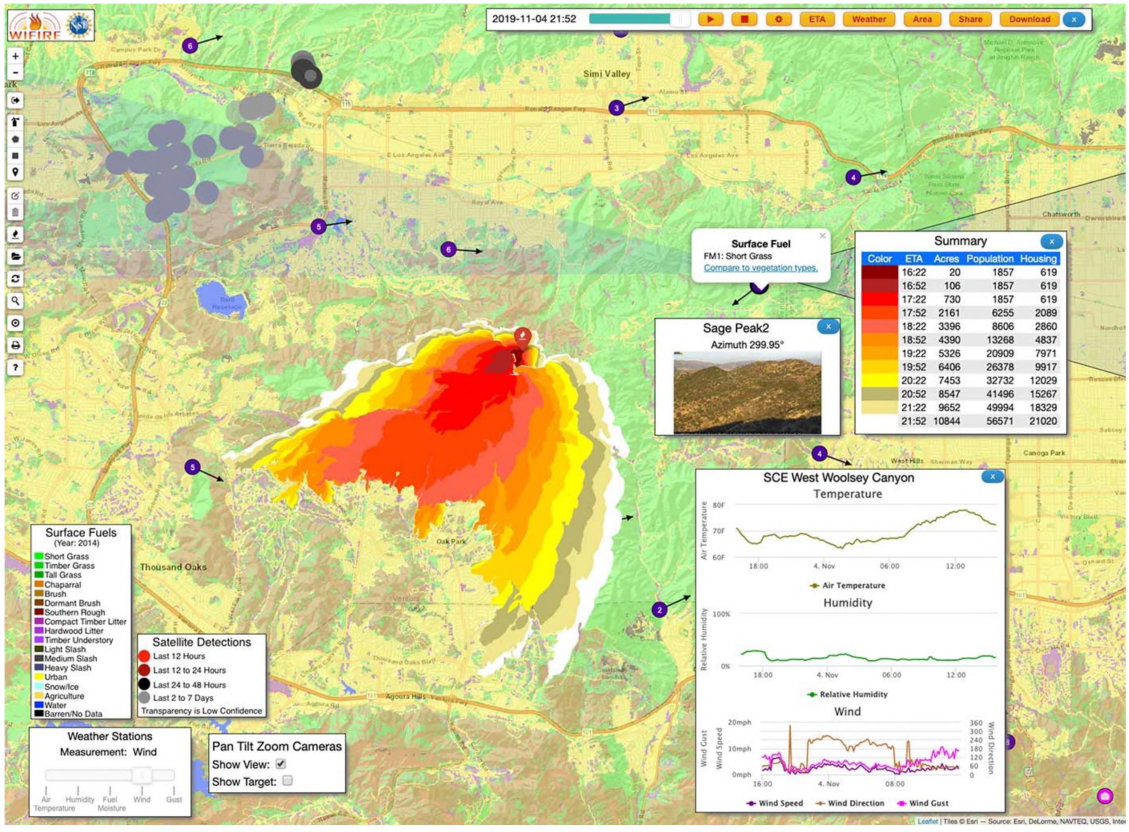

Figure 1.5. ALERTWildfire project in California U.S.

1.2. RELATED WORKS

Monitoring air quality especially tracers of wildfires emissions, such as particulate matter (PM) and carbon monoxide (CO) can be effective in identifying wildfire events. Air quality sensors are low-cost and sensitive to monitored gas species. They have low interference and they use scattering source and microprocessor for particle measurements [16]. Generally, air quality sensors work in three steps. In the first step, the sensors use laser scattering to radiate particles in the air. In the second step, the sensors collect the scattering light data over time. In the last step, the sensors use the built-in microprocessors to measure the particle concentrations, equivalent particle diameters, and number of particles with different diameters per unit volume. Figure 1.6 shows an air quality sensor that measures PM2.5 concentration [17].

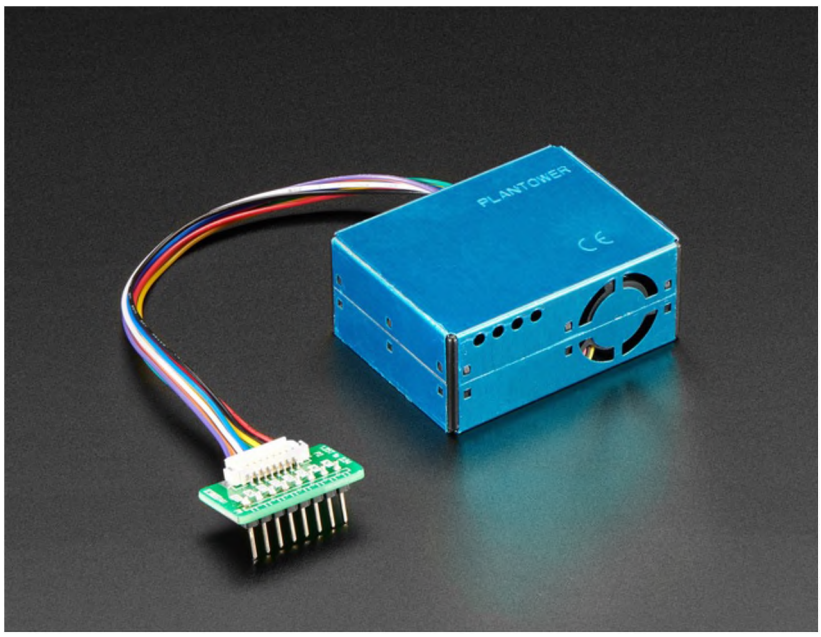

Figure 1.6. PM2.5 air quality sensor.

Existing work showed that common PM sensors achieved a low limit of detection [16]. By using a Kriging interpolation algorithm, the spatio-temporal distribution of PM can be mapped by a sensor network [18]. Conversely, low-cost CO sensors using triboelectric nanogenerators are available, and they can monitor CO concentrations without a battery by harvesting the movement of tree branches [19]. However, a challenge for using air quality sensors for wildfire detection is that an enormous number of sensors are required if they are deployed at fixed locations, thus, complicating data communication. Furthermore, it is difficult to deploy these sensors in hazard areas or forests.

The Unmanned Aerial Vehicle (UAV) is becoming a promising and realistic option for for wildfire detection and forest management because of its low cost, low maintenance, high mobility, and large coverage area including hazard areas (i.e., it can be operated in areas that cannot be accessed by humans or out of line-of-sight) [20, 21, 22, 23]. There are four types of UAVs being deployed by the National Interagency Fire Center (NIFC). Types 1 and 2 are complex systems requiring special personnel and designated areas for launching, and types 3 and 4 are simple devices (i.e., drones) that can be stored in backpacks and launched from fire lines [24].

Previous studies on optimizing the framework for wildfire detection mainly focused on using thermal imaging [8, 20, 21, 25, 26, 27]. These studies solved optimization problems to find the best watchtower locations that simultaneously minimized the cost and maximized the detection coverage. For instance, in [8], the authors proposed to build fixed watchtowers equipped with laser night vision and high-definition video cameras to monitor wildfires. More specifically, they formulated and solved an optimization problem to find the best watchtower locations that simultaneously minimized the cost and maximized the detection coverage. However, this solution was relatively costly and not dynamic. The work in [26] investigated the operational constraints, limitations, and opportunities for wildfire detection and monitoring of equipped UAVs with thermal camera image intensifiers. Although, there are various ranges of sensors can detect infrared radiation, each sensor has challenges, such

as considerable incident energy and reflected light during daytime, the dynamic behaviour of fire flame, and a need for advanced and accurate computer vision algorithms. The authors in [25] proposed a vision-based UAV system using color and motion features to process the captured images a UAV is flew. They first proposed a wildfire detection color algorithm to extract the fire-colored pixels using the chromatic feature. Then, the color algorithm was followed by flow algorithms to handle the effects of the UAV's vibration on the image quality. However, as mentioned earlier, thermal imaging may experience interference because the canopy and weather conditions.

Figure 1.7. Integrating the air quality sensors with the UAV.

Air quality sensors can be used to measure the concentration of fire emission signatures, such as PM and CO, that are the most affluent pollutants in fire emissions. The transport of air pollutants from combustion is not significantly affected by physical obstructions, therefore combining air quality sensors with UAVs can provide more accurate fire detection compared to imaging methods. Moreover, the detection limits of the sensors ~ 10 $\mu g\ m^{-3}$ for PM and ~ 0.5 ppm for CO [28] are far below the clean background conditions (~ 35 $\mu g\ m^{-3}$ for PM and ~ 35 ppm for CO) [29]. Recent studies show that integrating air quality sensors with UAVs could achieve faster responses to real fire events as shown in Figure 1.7 [30, 31]. Therefore, integrating the air quality sensors make a sensitive and early alarm system for wildfires [32]. Several studies considered designing sensors that measured both the CO and PM values [31, 33]. For instance, [31] shows that fire detection sensitiv-

ity was enhanced by measuring CO and PM values simultaneously with active sampling. Combining sensor integration of CO and PM with data processing algorithms can efficiently differentiate between real and nuisance fire sources, and thus reducing false alarms. In [34], Illingworth *et.al.* proposed using air-quality sensors equipped with large-scale Skywalker UAV. The authors showed how using UAVs for measuring the pollutant's concentration in sub-urban scale/areas can provide a useful additional indicator variability. This can lead to a better usage of air quality sensors equipped with UAVs in early detection of wildfires. Therefore, developing UAVs equipped with low cost air quality sensors can improve the wildfire detection paradigm for early detection and treatment. Table 1.1 compares the concerns for the established and proposed wildfire detection methods.

Table 1.1. Comparison between the main current and proposed wildfire methods.

Method	**Concerns**
Watchtowers	High labor cost. Safety issues for workers. Subject to delays in fire detection.
Satellite Remote Sensing	Limited spatial resolution. Observed area needs to be cloud-free.
Thermal Imaging	Limited resolution. Limited weather interference. Thick canopies may block the thermal signal from fire.
Air quality Sensors only	Needs to deploy large number of sensors to cover wide area Harder to be deployed in hazard areas or forests
Air quality + UAV	UAV battery limitation. Needs base station for tracking and communications.

Apart from fire detection, first responders require reliable communications when the existing communication capabilities during wildfires fail, therefore, from the public safety sector's perspective, enabling UAV technology with communication transceivers to send real-time data, including sensor readings and pictures, to nearby communications BSs. The data can be then analysed for the best course of action.

1.3. THESIS SCOPE AND CONTRIBUTIONS

This work focused on UAV types 3 and 4, due to their facile operation and routine usage in forest management. UAVs were previously employed to monitor progress of wildfires at low altitudes ($\leq$ 400 feet). However, their success in early-stage wildfire detection largely depends on the UAV patrol algorithm that determines the battery consumption and area of coverage in forest patrol [35]. Therefore, an efficient algorithm is needed to optimize the patrol of UAVs for accurate fire detection and efficient data communication, while maximizing forest patrol area.

Specifically, this work establishes the fundamentals of a UAV patrol algorithm for effective wildfire detection and forest management. It considered a UAV platform mounted with PM and CO sensors and equipped with the communication transceiver for data communication with the BSs. The main contributions of this work to the insight and design of energy efficient UAV patrolling systems for early wildfire detection were detailed in the following section.

In Section 2, the system model of wildfire detection based on integrated air quality sensors with the UAV was given. The contributions of this section were summarized as follows:

- Proposing the overall UAV patrolling and communication system model. This model included the patrolling flight pattern and communication links between the UAV and BSs. It was considered that communication BSs already existed.
- Discussing the pollutant dispersion model on the UAV patrolling problem.
- Discussing the UAV communications and data rate transmission channel gain on the communication problem.
- Showing the overall energy model that consisted of flying energy consumption and transmit energy consumption.

In Section 3, the UAV patrolling and communication mathematical problem was investigated. The contributions of this section were summarized as follows:

- Formulating an optimization problem that minimizes the total energy consumption while taking into consideration the detection threshold, achievable data rate quality, transmit power budget limitation, and the communication link associations between the UAV and BSs.
- Assuming that the UAV is transmitting different data types to selected BS simultaneously using orthogonal frequency division multiple access (OFDMA) technique. Each data type had certain throughput quality-of-service (QoS).
- Formulating two sub-problems: 1) Patrolling problem that optimized the UAV trajectory and patrolling horizontal gap, and 2) Communication problem that optimized the UAV-BS link associations in addition to the UAV transmit power when wildfire was detected.

In Section 4, the UAV patrolling solution was provided. More specifically, this section optimized the flight track of the UAV using a plume dispersion model to detect the wildfire tracer gas species with the goal of achieving wider areas of coverage for the UAV patrol and respecting the UAV battery limitations. The contributions of this section were summarized as follows:

- Analyzing the patrolling optimization problem by showing that the UAV patrolled at best altitude based on the pollutant dispersion model, thus reducing the 3D problem into 2D problem.
- Employing a meta-heuristic approach based on Genetic Algorithm (GA) to find a near optimal solution of patrolling horizontal gap due to non-convexity of the 2D problem.

- Analyzing the patrolling scheme's performance using Monte-Carlo simulation under various system parameters and different UAV's battery capacities. This study compared the proposed solution for different stability situations: very unstable, moderate unstable, slightly unstable, and neutral.

In Section 5, the UAV communication solution was provided. This section optimized communication resources and attempted to achieve the desired data rate QoS for each of data type. The contributions of this section were summarized as follows:

- Optimizing the communication link association between the UAV and BSs. By assuming the UAV was associated to one BS at a time. The study proposed to do the association with the best link.

- Proposing a software protocol to manage the resource allocation between the UAV and selected BS.

- Introducing loss-factor optimization to avoid the in-feasibility of transmit power allocation (i.e., in case the transmit power is not enough to achieve the data rate QoS).

- Solving the transmit power allocation and loss-factor optimization using convex methods.

- Illustrating the communication scheme's performance using Monte-Carlo simulation under different communication parameters and different transmit power budgets.

The conclusion was given in Section 6. Furthermore, two future directions were provided as potential extension of the work. The first recommendation is introducing a hotspot locations concept. This means based on historical wildfires data, some hotspot areas may need to be patrolled over them. The second suggestion is implementing directional communications, such as free-space-optical (FSO) communications, for data transmission where FSO link can reach few kilometers coverage, in addition to the capability of high speed data rates. This can be helpful in extending the communication coverage area.

2. SYSTEM MODEL

This section proposed the system model. The system model consisted of one UAV patrolling over a rectangular-shaped flat area covered by forest. The UAV was equipped with a communication transceiver to communicate with one of the L nearby communication BSs when a wildfire was detected as shown in Figure 2.1. The area had a pre-defined wind direction of θ_w (as a reference, $\theta_w = 0$ is pointing north). In addition, the UAV was equipped with air quality sensors monitoring the concentrations of PM (μgm^{-3}) and CO (ppm).

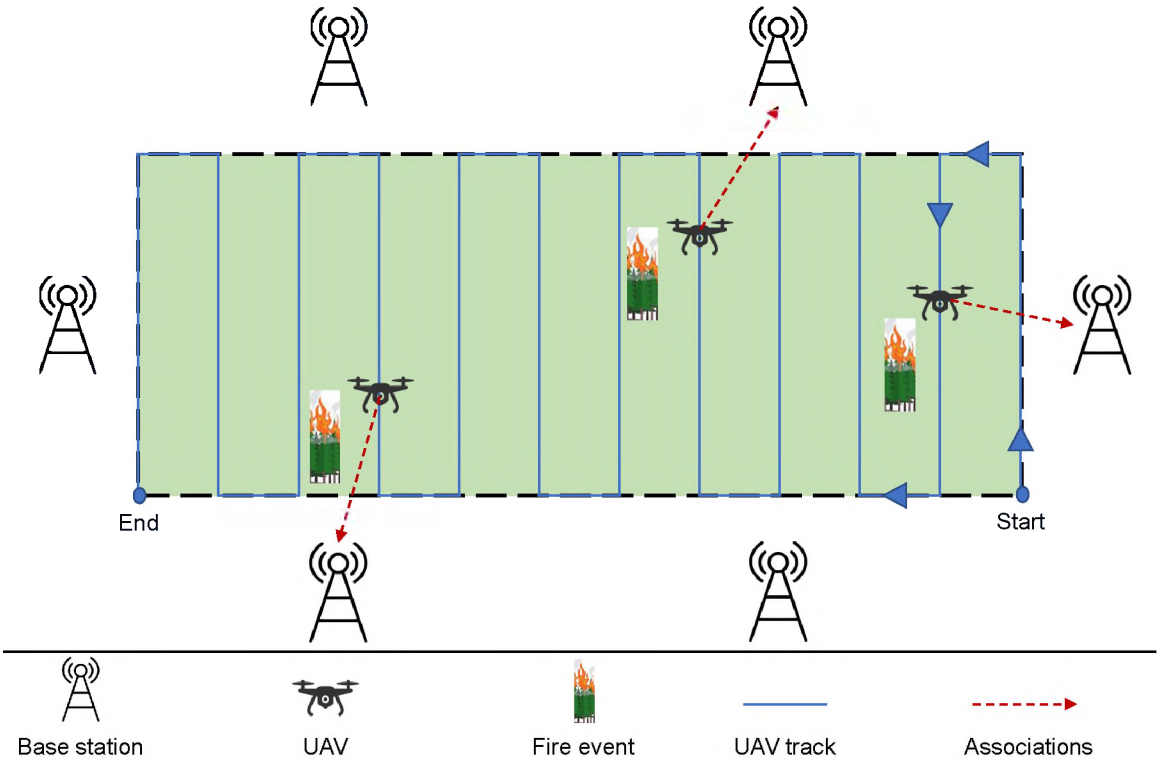

Figure 2.1. System model.

A wildfire event were identified when the air pollutant concentrations measured by both sensors were above the forest backgrounds [36]. Then, the UAV transmitted real-time data to a selected BS. It was assumed that an early-stage wildfire happened at a random

location in the patrolled area and continuously emited PM and CO pollutants in to the environment via a plume that transported with the wind and dispersed in all directions, as shown in Figure 2.2. To effectively detect and report wildfire events, the following four parameters were optimized: (1) the altitude of the UAV that ensured the UAV transected the plume; (2) the flight pattern of the UAV that ensured the UAV samples were in the plume for a considerable time; (3) the link association or the communication link between the UAV and BSs, and (4) the UAV's transmitted power of data communication to the selected BS. These four parameters affected battery and energy consumption and determined the total distance traveled by the UAV and the area of coverage.

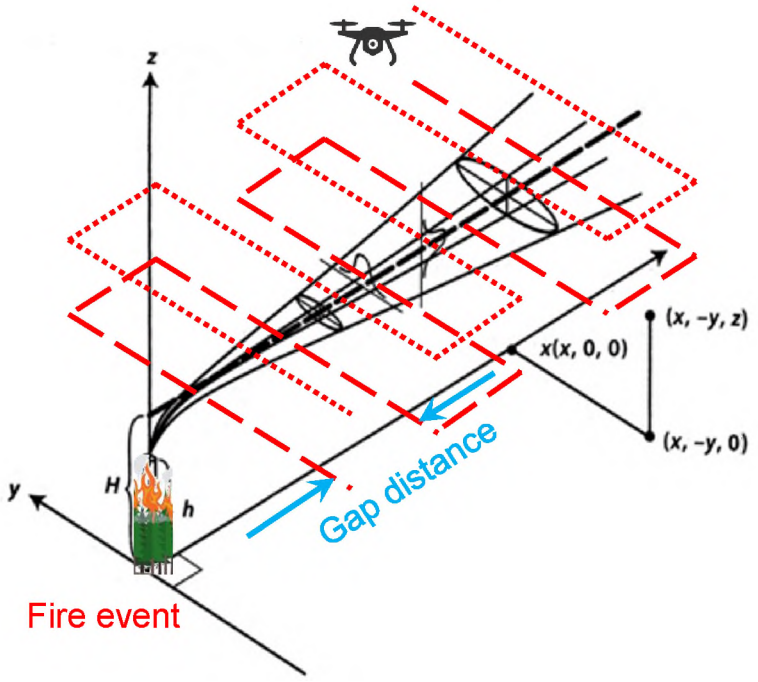

Figure 2.2. A schematic diagram of the Gaussian dispersion model for predicting the air pollutants concentrations in a plume.

2.1. POLLUTANT DISPERSION MODEL

The UAV's speed is V; therefore, $V\hat{T}$ is the maximum distance that the UAV can travel every time slot t, where $\hat{T}$ is the time slot duration. The location of the UAV were considered as 3D coordinates during a time slot t as $\hat{U}[t] = (x[t], y[t], z[t])$. It was assumed that the UAV was initially in a Start Point location and that it would land at the End Point location after finishing the investigation, as shown in Figure 2.1.

The transport of the plume is typically described by dispersion models [29]. The most widely used model that predicts the transport of air pollutants in a plume is the Gaussian dispersion model, as shown in Figure 2.2, where the concentration of air pollutants emitted from an elevated source can be calculated by [29]:

$$C(x,y,z) = \frac{Q}{2\pi u \sigma_y(x)\sigma_z(x)} \exp\left(-\frac{y^2}{2\sigma_y^2(x)}\right)\left[\exp\left(-\frac{(z-H)^2}{2\sigma_z^2(x)}\right) + \exp\left(-\frac{(z+H)^2}{2\sigma_z^2(x)}\right)\right] \tag{2.1}$$

where C is the steady-state concentration at a point (x, y, z), Q is the emission rate, $\sigma_y(x)$ and $\sigma_z(x)$ are the horizontal and vertical spread parameters, respectively, depending on the atmospheric stability and function of distance x. Note that u is the average wind speed, z is the vertical distance from the plume centerline, and H is the effective height of the emission point.

For simplicity, this study uses the index $i = \{1, 2\}$ to refer to PM and CO index, respectively. Similarly, the sensor concentrations are given as C_1 and C_2 for the concentration of PM and CO, respectively. A binary variable $\rho_i[t]$ is introduced to indicate if the concentration of pollutant i exceeds the concentration threshold $C_{th,i}$ during time t:

$$\rho_i[t] = \begin{cases} 1, \text{ if } C_i[t] \geq C_{th,i} \text{ during time slot } t \\ 0, \text{ otherwise.} \end{cases} \tag{2.2}$$

By defining $\bar{C}_i$ as the maximum concentration value of pollutant i (the value which can be measured exactly at the fire point), (2.2) can be written as an equivalent mathematical expression as follows:

$$(C_{th,i} - C_i[t]) - \bar{C}_i(1 - \rho_i[t]) \leq 0, \quad \forall i, \forall t, \tag{2.3}$$

and

$$(C_i[t] - C_{th,i}) - \bar{C}_i\rho_i[t] \leq 0, \quad \forall i, \forall t. \tag{2.4}$$

Note that employing both constraints (2.3) and (2.4) are necessary to represent (2.2) in mathematical equations. For simplicity, assume $\rho[t] = \rho_1[t]\ \rho_2[t]$, where $\rho[t]$ equals 1 if the concentrations for both pollutants are greater that concentration threshold and 0 otherwise (i.e., the concentration of one pollutant is less than the threshold).

2.2. UAV COMMUNICATIONS CHANNEL MODEL

As discussed in [37], the BS can receive two different types of communications signals in addition to the line-of-sight signal. The first type is strong reflected non-line-of-sight, and the second type consists of multi reflected fading signals. Both non-line-of-sight signal types can be considered independently with different probabilities of occurrences (i.e, the probabilities of line-of-sight occurrences) for each type [37]. Probabilities of occurrences depend on various factors such as density, obstacles dimensions, transmission elevation angles. The probability of multiple reflections was assumed to be negligible compared to the line-of-sight signal and strong reflected non-line-of-sight [37, 38]. One of the common technique that characterizes the UAV to BS channel gain is modeling the ground-to-air Path Loss (PL) using line-of-sight and non-line-of-sight components with their separate probabilities of occurrences. In other words, the channel gain was considered as a weighted the sum of the two PLs links (i.e., line-of-sight signal and strong reflected non-line-of-sight links) [37, 39].

Therefore, the probability of line-of-sight between the UAV and the BSs can be obtained. Hence, the PL between UAV and BS l positioned at a location $\hat{U}[t]$ for line-of-sight signal and strong reflected non-line-of-sight are given, respectively, as follows [37, 40, 41]:

$$PL_l^{\text{LoS}}[t] = \xi_{\text{LoS}} \left(\frac{4\pi\zeta_l[t]}{\lambda_0} \right), \tag{2.5}$$

$$PL_l^{\text{NLoS}}[t] = \xi_{\text{NLoS}} \left(\frac{4\pi\zeta_l[t]}{\lambda_0} \right), \tag{2.6}$$

where $\zeta_l[t] = ||\hat{U}[t] - \hat{U}_l||$ is the distance between the UAV, and BS l and $\hat{U}_l$ is the fixed location of BS l, and λ_0 is the wavelength of the radio signal. Note that ξ_{LoS} and ξ_{NLoS} are the additional shadowing losses to the free space propagation for line-of-sight signal and strong reflected non-line-of-sight links, respectively. The line-of-sight probability is [42]:

$$p_l^{\text{LoS}}[t] = \frac{1}{1 + \nu_1 \exp(-\nu_2[\Theta_l[t] - \nu_1])}, \tag{2.7}$$

where $\Theta_l[t] = \frac{180}{\pi} \sin^{-1}\left(\frac{z[t]}{\zeta_l[t]}\right)$ is the elevation angle between the UAV and BS l in degree. Note that ν_1 and ν_2 are constant values that depend on the environment. Thus, the strong reflected non-line-of-sight probability is equal to $1 - p_l^{\text{LoS}}[t]$. Based on this PL model, the average PL for ground-to-air link is given by:

$$\text{PL}_l[t] = p_l^{\text{LoS}}[t] PL_l^{\text{LoS}}[t] + (1 - p_l^{\text{LoS}}[t]) PL_l^{\text{NLoS}}[t]. \tag{2.8}$$

Finally, the average channel gain between the UAV and BS l during time slot t is given by:

$$g_l[t] = \frac{1}{\text{PL}_l[t]}. \tag{2.9}$$

2.3. DATA TRANSMISSION

It was assumed that wildfire was detected when both PM and CO concentrations rose above their concentration thresholds. Therefore, the UAV had to transmit real-time data to the selected BS. The data types were categorized into different $n = 1, .., N$ types based on QoS, which was given as data rate threshold $R_{th,n}$ in bits/s. In addition to the air-quality sensors, this study assumed that the UAV was equipped with a thermal camera taking pictures or videos to increase decision accuracy. For example, the QoS of the sensor readings defer from the QoS of the thermal pictures or videos. Note that, different QoS data was referenced as a separate data type.

A binary variable $\epsilon_l[t]$ is introduced to indicate the communication link association between the UAV and BS l during time slot t. It equals 1 if the UAV is associated with BS l during time slot t, and 0 otherwise, and is calculated by:

$$\epsilon_l[t] = \begin{cases} 1, \text{ if the UAV is associated with BS } l \text{ during time slot } t \\ 0, \text{ otherwise.} \end{cases} \tag{2.10}$$

The goal was to transmit all data types to the selected BS if both pollutants concentration were greater than the threshold (i.e., $\rho[t] = 1$) Therefore, the data rate of each transmitted data type n is aiming to satisfy the following condition:

$$\rho[t]\epsilon_l[t]\left(B_0 \log_2\left(1 + \frac{P_n[t]g_l[t]}{B_0 N_0}\right) - R_{th,n}\right) \geq 0, \quad \forall n, \forall l, \forall t \tag{2.11}$$

where $P_n[t]$ and $g_l[t]$ are the UAV's transmit power allocated for data type n and channel gain between the UAV and BS l during time slot t, respectively. Note that B_0 and N_0 are the communication bandwidth and the noise power, respectively. Constraint (2.11) indicates that the UAV had to transmit all data types, thus satisfying the QoS condition when the wildfire was detected (i.e., $\rho[t] = \rho_1[t]\ \rho_2[t] = 1$), and it did not transmit when there

is no wildfire (i.e., $\rho[t] = \rho_1[t]\ \rho_2[t] = 0$). In other words, $\rho[t] = 1$ only when both concentrations are above the threshold, and $\rho[t] = 0$ if at least one of the concentration is below the threshold.

2.4. UAV ENERGY MODEL

The UAV consumed operation and communication transmission energies. The UAV communication transmitted power can be given as [43]:

$$P_C[t] = \sum_{n=1}^{N} P_n[t], \tag{2.12}$$

where $P_C[t]$ and $P_n[t]$ are the total UAV's communication power and transmit power of data type n during time slot t. In addition to the transmit power, the UAV consumed flying and hovering powers $P_F[t]$, and is given as [44]:

$$P_F[t] = \left(\sqrt{\frac{(m_{\text{tot}}G)^3}{2\psi r_p^2 \omega_p \psi}} + P_s \right) \tag{2.13}$$

where P_s denotes the consumed power due to UAV hardware in (W), ψ is the air density in (kg/m^3), G is the earth gravity in (m/s^2), and m_{tot} the UAV mass in (kg). Parameters ω_p and r_p respectively donate to the number of the UAV propellers and to the UAV radius of the UAV. Therefore, the total energy consumption can be given as:

$$E_{tot} = E_F + E_C = \hat{T} \sum_{t=1}^{T} P_F[t] + \hat{T} \sum_{t=1}^{T} P_C[t]. \tag{2.14}$$

Note that because $E_F >> E_C$ (power consumption of multiple Watts for flying compares to fractional Watts for transmission), the total energy in (2.14) can be approximated as [43, 44]:

$$E_{tot} \approx E_F = \hat{T} \sum_{t=1}^{T} P_F[t], \tag{2.15}$$

where T is a dependent variable that can effect the total energy; for example, if the patrol UAV finished the patrolling trip early, then T becomes smaller, and the energy will be lower. Note that, although $P_C[t]$ is much smaller than $P_F[t]$, there was a need to optimize it because the transmitted power plays a significant role in satisfying the data QoS given in (2.11). The effect of the $P_C[t]$ in the communication optimization problem was shown in Section 5.

3. UAV PATROLLING AND COMMUNICATION OPTIMIZATION

In this section, the UAV patrolling and communication mathematical problem was formulated. The goal was to minimize the total energy consumption and satisfy the detection threshold, achievable data rate quality, transmit power budget, and the UAV and BSs communication link associations constraints. Furthermore, it was assumed that the UAV could transmit different data types at the same time over different bandwidths or frequencies using the OFDMA technique.

The optimization problem was formulated to minimize the UAV's total energy during all time slots, while trying to satisfy certain QoS for each data type when detecting a wildfire. Also, two complementary sub-optimization problems were formulated. The goal for the first one was to find the optimal UAV trajectory within the desired area. The second optimization problem optimized the association between UAV and BSs, and the UAV transmitted allocated power for each data type when the wildfire was detected.

Minimizing the UAV's energy consumption was achieved by minimizing the UAV's travel time when reaching $C_{th,i}$, $\forall i = \{1, 2\}$ and detecting wildfire. This was done by optimizing the UAV's trajectory. Due to the limited battery of the UAV, the flight track of the UAV determined the area that UAV patrolled. For simplicity, it was assumed that the UAV adopted rectangular track, as shown in Figure 3.1. With this rectangular flight track, the total distance traveled by the UAV was strongly affected by the distance between the two parallel legs named horizontal gap and given by Δx. A narrower gap led to longer flight distances and faster battery consumption, and a wider gap led to ineffective wildfire tracer detection and lower energy consumption. Note that this rectangular track with Δx optimization could be modified easily for other tracks, such as square or spiral tracks. The rectangular track was chosen for simplicity.

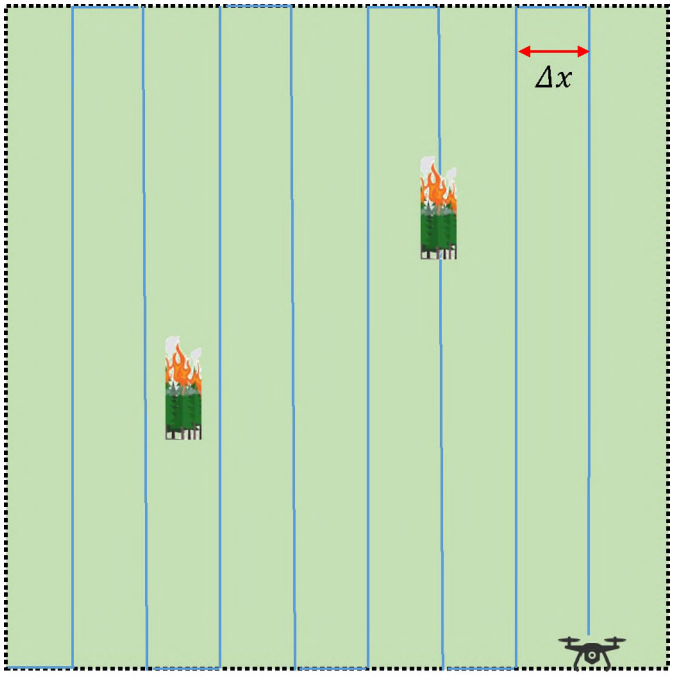

Figure 3.1. A schematic diagram of the studied problem. The optimization of the UAV patrol algorithm should identify an optimal flight track for the effective detection of wildfire events.

3.1. GENERAL OPTIMIZATION PROBLEM

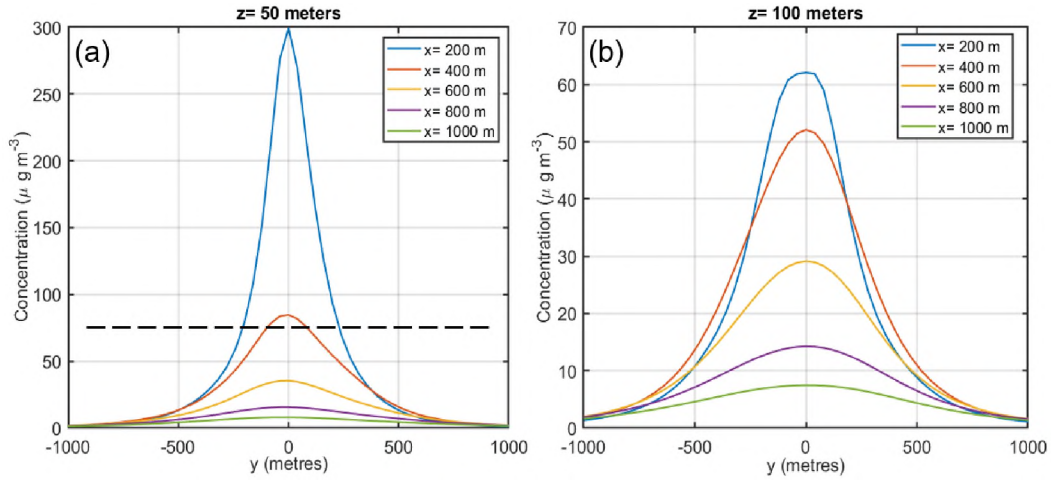

Figure 3.2. The profile PM concentrations along the y axis at different distances (x) downstream of the emission point at an altitude (z) of (a) 50m and (b) 100m, according to the Gaussian dispersion model.

Figure 3.2 shows the profile of PM concentrations along the parallel legs at different distances downstream of a fire event using emission factor equal to 20g/kg fuel [36]. Figure 3.2 also compares the profile of PM concentrations at different UAV's altitudes (i.e., z = 50m z = 100m). For instance, when using $75\mu g$ m^{-3} as the threshold of PM measurement based on three times of the regulated concentration to identify the fire event for z = 50m [29, 45], the PM concentrations above the threshold will only occur within around 400m downstream of the fire event as shown in Figure 3.2-a. This means that that a UAV using a gap distance wider than 400m may not be able to detect the fire event during the patrol. For z = 100m, Figure 3.2-b shows that if the UAV is not maintained at an ideal altitude, the UAV will miss the fire event even at 200m downstream the fire. This study used the Gaussian dispersion model to calculate the maximum gap distance of the UAV. Based on the battery capacity of common UAVs, the maximum distance that can be traveled by the UAV and the area of the forest that can be patrolled were calculated.

The general optimization problem was aiming to minimize the total UAV's energy during all time slots, while satisfying certain QoS when detecting wildfire. The optimization variables are: i) the UAV altitude, ii) the UAV pattern or horizontal gap, iii) the association between the UAV and BSs, and iv) the UAV transmitted power for each data type. Therefore, the proposed optimization problem can be formulated as:

$$\underset{(z[t],y[t],\Delta x,P_n[t])\geq 0,(\rho_i[t],\epsilon_l[t])\in\{0,1\}}{\text{minimize}} \quad E_{tot} \tag{3.1}$$

subject to

$$(C_{th,i} - C_i[t]) - C_{th,i}(1 - \rho_i[t]) \leq 0, \quad \forall i, \forall t \tag{3.2}$$

$$(C_i[t] - C_{th,i}) - \bar{C}_i\rho_i[t] \leq 0, \quad \forall i, \forall t \tag{3.3}$$

$$\rho[t] = \prod_{i=1}^{2} \rho_i[t], \quad \forall t, \tag{3.4}$$

$$\rho[t]\epsilon_l[t]\left(B_0 \log 2\left(1+\frac{P_n[t]g_l[t]}{B_0 N_0}\right)-R_{th,n}\right)\geq 0, \quad \forall n, \forall l, \forall t, \tag{3.5}$$

$$\sum_{n=1}^{N} P_n[t] \leq \bar{P}, \quad \forall t, \tag{3.6}$$

$$\sum_{l=1}^{L} \epsilon_l[t] \leq 1, \quad \forall t, \tag{3.7}$$

where constraints (6.4) - (6.7) are to ensure that when wildfire is detected, the variable parameter $\rho[t]$ is equal to 1. Constraint (3.5) is to guarantee a certain QoS ($R_{th,n}$) for each data type. Constraint (3.6) presents transmit power limitation due to transmitters' hardware capabilities. Constraint (3.7) is to guarantee that the UAV can be connected to one BS at most at a time t. In the sequel, the details of the two trajectory and communications sub-problems were provided.

3.2. TRAJECTORY OPTIMIZATION

To effectively detect early-stage fire events, the UAV needs to optimize its altitude and trajectory. Therefore, the patrolling optimization sub-problem can be given as

$$\underset{(z[t],y[t],\Delta x,)\geq 0,}{\text{minimize}} \quad E_{tot} \tag{3.8}$$

subject to

$$C(x=\Delta x, y[t], z[t]) \geq C_{th,i}, \quad \forall i, \tag{3.9}$$

where constraint (3.9) is to insure that the horizontal spacing Δx, $y[t]$, and $z[t]$ takes into account satisfying $C_{th,i}$ for both PM and CO pollutant species in case of a wildfire happened in area of interest. This is to ensure to detect the wildfire anywhere in the area of interest. Note that value of $\rho[t]$ will be based on a real-time concentration measurement of PM and CO sensors.

3.3. DATA TRANSMISSION OPTIMIZATION PROBLEM

In this section, the data transmission sub-problem were formulated, while accounting the QoS constraint given in (3.5) when a wildfire was detected (i.e., when $\rho[t] = 1$). Therefore, the communication sub-problem that optimized the UAV transmit power for each data type $P_n[t]$ and communication link associations $\epsilon_l[t]$ is given as:

$$\underset{P_n[t]\geq 0, \epsilon_l[t]\in\{0,1\}}{\text{minimize}} \quad E_{tot} \tag{3.10}$$

subject to

$$\rho[t]\epsilon_l[t]\left(B_0 \log 2\left(1+\frac{P_n[t]g_l[t]}{B_0 N_0}\right)-R_{th,n}\right)\geq 0, \quad \forall n, \forall l, \forall t, \tag{3.11}$$

$$\sum_{n=1}^{N} P_n[t] \leq \bar{P}, \quad \forall t, \tag{3.12}$$

$$\sum_{l=1}^{L} \epsilon_l[t] \leq 1, \quad \forall t. \tag{3.13}$$

4. UAV PATROLLING SOLUTION

In this section, the solution of the UAV patrolling optimization sub-problem was proposed. This section optimized the flight track of the UAV using a plume dispersion model to detect the wildfire tracer gas species with the goal of achieving a wider area of coverage for the UAV patrol and respecting the UAV's battery limitations. Furthermore, this section illustrated Monte-Carlo simulation results to validate the feasibility of the solution.

To effectively detect early-stage fire events, the UAV must transect the plume at the altitude of the plume centerline $z[t] = H$; which it can be calculated by [29]:

$$H = h_0 + \frac{v_s d_s}{u}\left[1.5 + 2.68 \times 10^{-2} P_a . \left(\frac{K_s - K_a}{K_s}\right) d_s\right] \tag{4.1}$$

In (4.1), h_0 is the height of the plume on fire, v_s is the upward velocity of the plume, d is the diameter of the plume at the emission point, P_a is the pressure, K_s is the temperature of the plume, and K_a is the ambient air temperature. In addition, based on the Gaussian dispersion model, the maximum concentration will happen when $y = 0$, as shown in Figure 3.2. Therefore, based on the ambient condition and existing data characterizing fire plumes [46], the optimal/maximum horizontal spacing distance Δx of the rectangular UAV motion can be calculated, as shown in Figure 3.1, by solving the following optimization problem; note that maximizing Δx is equivalent to minimizing E_F:

$$\underset{\Delta x}{\text{maximize}} \quad \Delta x \tag{4.2}$$

subject to:

$$C(x = \Delta x, y = 0, z = H) \geq C_{th,i}, \quad \forall i, \tag{4.3}$$

where constraint (4.3) is to ensure that the horizontal spacing Δx satisfies $C_{th,i}$ for all pollutant species (i.e., PM and CO). Next, this study proposed a solution to solve the formulated optimization problems given in (4.2)-(4.3) by using genetic algorithm (GA).

4.1. TRAJECTORY OPTIMIZATION SOLUTION

The problem formulated in (4.2)-(4.3) is a non-convex and non-linear optimization problem. Therefore, it was difficult to find the optimal solution [47]. Hence, it was proposed to use a GA to find a sub-optimal solution to the problem. This algorithm depends essentially on random-natural evolution. Initially, GA generated a random population set containing a set number of strings. For each generation, the strong strings survived the algorithm; whereas, the weak ones died. After that, the GA generated new strings from the surviving strings using mutation and crossover operations [48].

4.1.1. GA Coding Approach. In the GA coding approach, it was proposed to divide the horizontal spacing distance Δx into δ quantization levels between 0 and $\bar{x}$, as follows: $\left(\Delta x \in \left\{0, \frac{\bar{x}}{\delta-1}, \frac{2\bar{x}}{\delta-1}, ..., \frac{(\delta-2)\bar{x}}{\delta-1}, \bar{x}\right\}\right)$, where $\bar{x}$ is the maximum horizontal spacing distance. Therefore, Δx could be one of the levels between 0 and $\bar{x}$.

Note that to employ the GA approach, Δx levels had to be encoded into binary words b. The length of the binary words b depended on δ (i.e., the number of quantization levels) as follows: $\text{length}(b) = \lceil \log_2 \delta \rceil$, where $\lceil . \rceil$ denotes the integer round towards $+\infty$. For example, if $\delta = 4$, then two bits are sufficient to encode these levels. If $\delta = 17$, then five bits are needed. In the latter case, the required words were less than a power of 2. This was because some binary words were redundant, and they corresponded to any valid word. Several solutions were proposed to solve this problem by discarding these words as illegal, then by assigning them a low utility or mapping them to a valid word with fixed, random, or probabilistic remapping [49].

Algorithm 1 Proposed Genetic Algorithm

- **Initialization:** $\Delta x = 0$.
- Generate a random initial population containing all S_j, $\forall j = 1, \cdots, S$.
- iteration $it = 1$

while (not converge or $it \leq$maximum iteration:) **do**
  for $j = 1 : S$ **do**
    - Find $\Delta x_j(it)$ corresponding to the string S_j, $\forall j = 1, \cdots, S$ for iteration it.
    if constraint (4.3) is satisfied **then**
      - $\Delta x_j(it) = \Delta x_j(it)$
    else
      - Set $\Delta x_j(it)$ to 0.
    end if
  end for
  - Save $\Delta x(it)$ such that $\Delta x(it) = \max_j \quad \Delta x_j(it)$.
  - Keep the best τ strings, thus providing the highest $\Delta x_j(it)$ to the next population.
  - From the survived parents (τ strings), generate $S-\tau$ new strings by applying crossovers and mutations to generate a new population set.
  - $it = it + 1$.
end while
- Find optimal Δx^* such that $\Delta x^* = \max_{it} \quad \Delta x(it)$.

4.1.2. GA Approach. The GA approach was started by randomly generating S binary strings to formulate the initial population set. Each string S_j, $\forall j = 1, \cdots, \bar{S}$ had a binary word and built by b corresponding to the Δx levels (an example of 4 strings and 8 binary word length is shown in Figure 4.1). Then the GA algorithm computed Δx_j that corresponded to S_j after verifying whether the constraint (4.3) was satisfied or not. After that, the algorithm selected the best τ strings (where $1 \leq \tau \leq S$) that provided the highest Δx to keep them to the next population cycle (called survived parents strings). Conversely, the algorithm applied GA operations that consisted of crossover and mutation operations on the survived parents to formulate new $S - \tau$ (called children strings). Note that crossover operation consisted of i) dividing two survived parents strings at a random point, and ii) swapping the obtained fragments to recombine and produce two new children strings. The mutation operator was used by changing a random string value with probability p (an

example of crossover and mutation operation is shown in Figure 4.2). This GA procedure was repeated until convergence or until a maximum generation pre-defined number was reached.

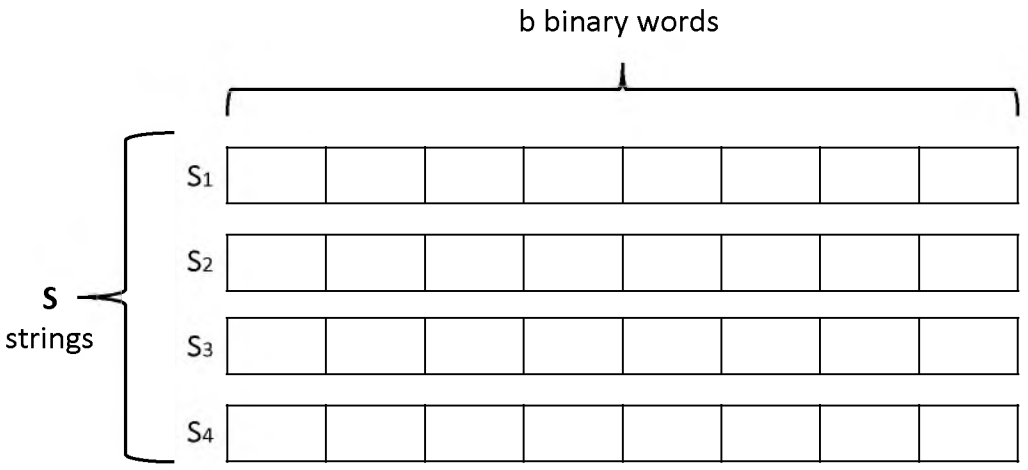

Figure 4.1. GA approach example with 4 strings and 8 binary word length.

The proposed GA with discrete levels is detailed in Algorithm 1.

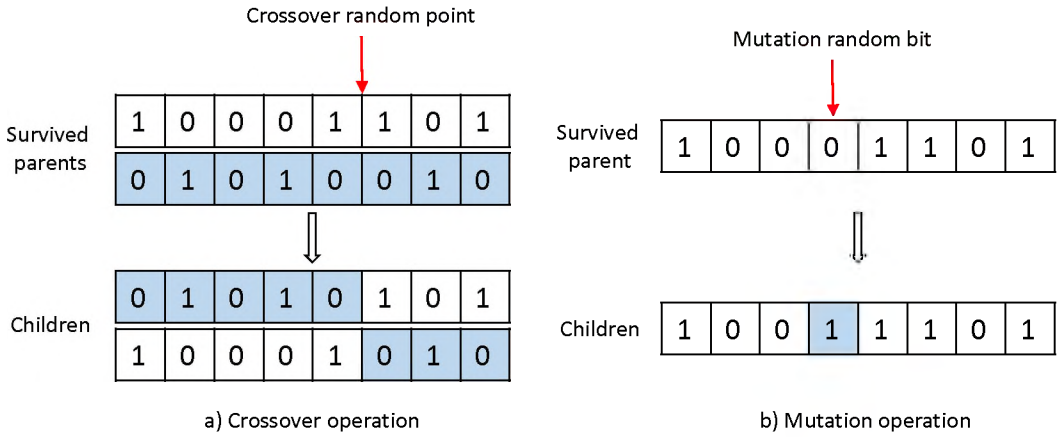

Figure 4.2. GA operations example.

4.2. PATROLLING SIMULATION RESULTS

This section presented simulation results to illustrate the proposed solution. The study considered the reference emission rate $Q_{0,i}$ of the PM and CO following Gaussian distribution $\mathcal{N}(17.4, 7.2)$ and $\mathcal{N}(64.5, 16.7)$, respectively [36]. It was assumed that $C_{th,1}$ and $C_{th,2}$ were equal to 75μg/m^3 and 150ppm (based on three times of the regulated concentration to identify the fire event) [29, 45]. The rest of the simulation parameters are summarized in Table 4.1 [29, 50, 51]. Four stability situations (very unstable, moderate unstable, slightly unstable, and neutral) were considered based on the dispersion model given in (2.1). In other words, σ_y and σ_z were calculated based on reasonable approximated fit and given, respectively, as [29]:

$$\sigma_y = ax^b, \tag{4.4}$$

$$\sigma_z = cx^d + f, \tag{4.5}$$

where the parameters a, b, c, d, f are given in Table 4.2 [29]. Figure 4.3-Figure 4.5 show examples of 2D Gaussian pollutants concentrations dispersion model in a plume for very unstable, slightly unstable, and neutral atmospheric stability situations, respectively.

Table 4.1. Patrolling simulation parameters.

Constant	**Value**	**Constant**	**Value**	**Constant**	**Value**
V [m/s]	5	h_0 [m]	15	v_s [m/s]	1.55
d_s [m]	4.75	K_a [K]	308.15	K_s [K]	1106.15
P_a [mb]	1000	P_s [W]	0.5	m_{tot} [kg]	1
ψ [kg/m^3]	1.225	ω_p	4	r_p	0.2

Figure 4.6 plots the horizontal gap Δx as a function of wind speed u. It was shown that as the wind speed increased, the horizontal gap decreased for all different types of stability situations. This was because the relationship between pollutant concentration C and wind speed u was inverse propositional, as given in (2.1). Note that when C at the

same location (x, y, z) increased, then Δx increased because the UAV was able to detect the C_{th} beyond this point. For low wind speed values, the gaps between different types of stability situations were large. For example, when $u = 2$[m/s], Δx for neutral and very unstable situations were approximately 220m and 160m, respectively, with an approximate difference of 80m. When $u = 20$[m/s], Δx for neutral and very unstable situations were about 900m and 400m, respectively, with difference of about 500m. As u increased, the gap between the different stability situations was reduced.

Table 4.2. Stability coefficients based on the Gaussian dispersion model.

			$\Delta x \leq$ 1km			$\Delta x >$ 1km		
Stability	**a**	**b**	**c**	**d**	**f**	**c**	**d**	**f**
1- Very unstable	213	0.894	440.8	1.941	9.27	459.7	2.094	-9.6
2- Moderate unstable	156	0.894	106.6	1.149	3.3	108.2	1.098	2.0
3- Slightly unstable	104	0.894	61.0	0.911	0	61.0	0.911	0
4- Neutral	68	0.894	33.2	0.725	-1.7	44.5	0.516	-13.0

Figure 4.7 illustrates the horizontal gap Δx versus the emission rate factor κ. The factor κ is defined as a parameter to express the emission rate, in terms of the the reference emission rate, as $Q_i = \kappa_i Q_{0,i}$, $\forall i = \{1, 2\}$. Note that the emission rate factor for PM2.5 and CO are denoted as κ_1 and κ_2, respectively. This helped show the effect of the increase or decrease in emission rates on the horizontal gap. As shown in Figure 4.7, for the same emission rate factor $\kappa = \kappa_1 = \kappa_2$, as κ increased, the horizontal gap increased. This confirmed the proportional relationship between C and Q in (2.1). Thus, Δx increased when Q increased.

Figure 4.8 and Figure 4.9 illustrate the horizontal gap Δx by fixing one emission rate factor and changing the other for very unstable and neutral situations. For instance, in Figure 4.8 κ_1 varied and κ_2 was fixed for both very unstable and neutral situations. In other words, the Q_1 varied and Q_2 was fixed. For low values of κ_1, the PM pollutant was dominant for Δx optimization up to the cut-off point (i.e., around 1.5 for very unstable

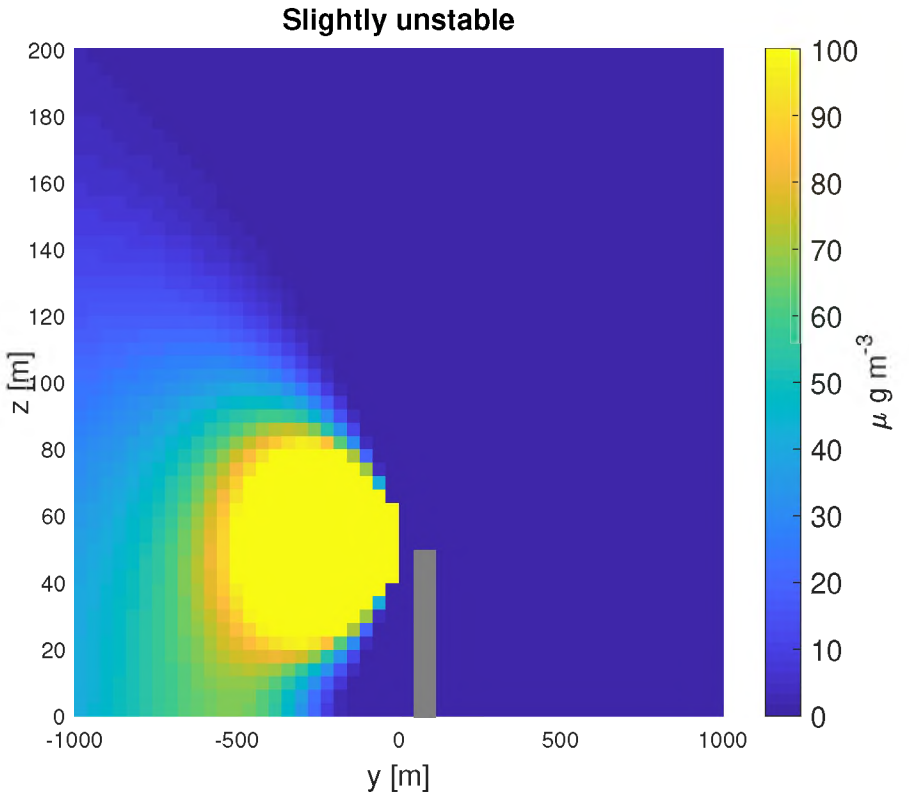

Figure 4.3. 2D Gaussian pollutants concentrations dispersion model in a plume for slightly stability situation.

situation and 1.25 for neutral situation). After that, the CO pollutant was the dominant factor in Δx optimization. In Figure 4.9, κ_2 varied and κ_1 was fixed for both very unstable and neutral situations. Meaning, the emission rate of CO varied and the emission rate of PM2.5 was fixed. In this case, the study yielded different cut-off points (i.e., around 0.5 for very unstable situation and 0.8 for neutral situation).

Figure 4.10 showed the expected rectangular area that UAV with a velocity V = 5[m/s] can be patrolled as a function of horizontal gap for different battery capacities. It was shown that as horizontal gap increased and the patrolled area is also increased. For example, with horizontal gap Δx = 500m, the UAV can cover areas of approximately 1km^2 and 3.2km^2 with battery capacities of 6KJ and 24KJ, respectively.

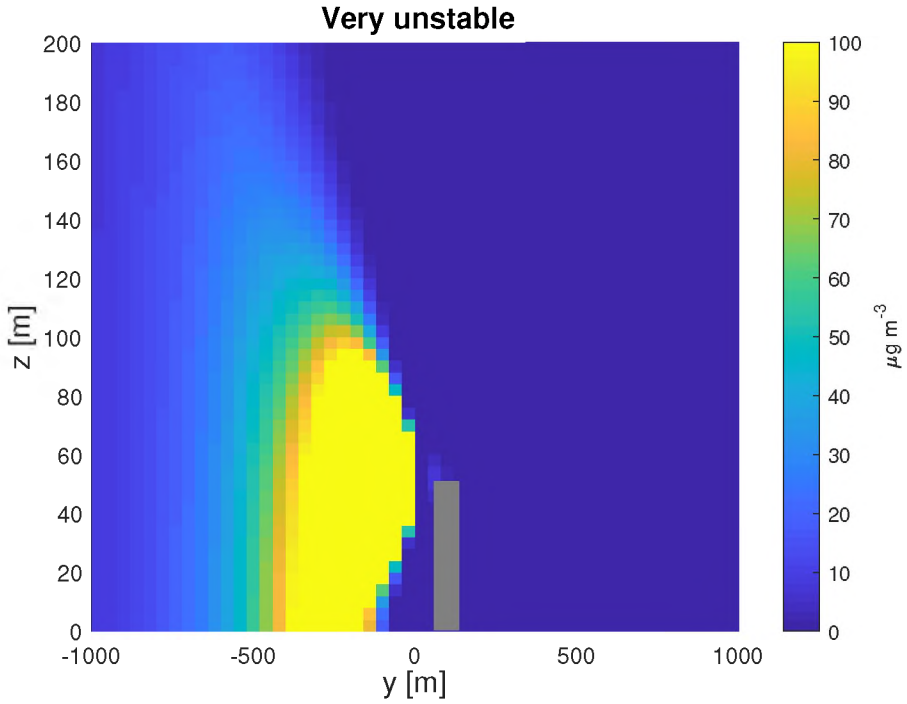

Figure 4.4. 2D Gaussian pollutants concentrations dispersion model in a plume for very unstable stability situation.

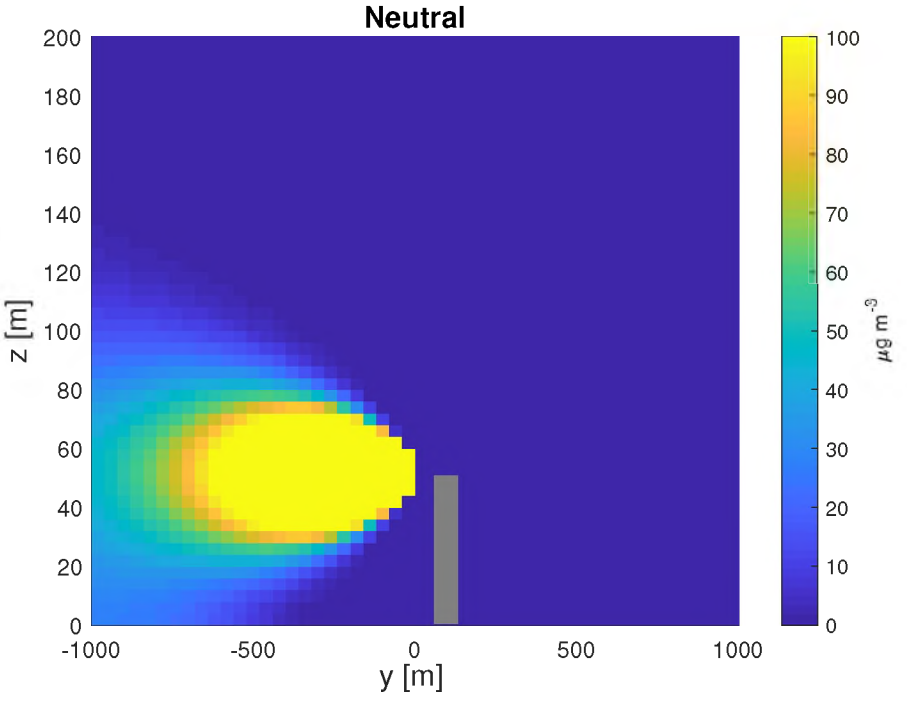

Figure 4.5. 2D Gaussian pollutants concentrations dispersion model in a plume for neutral stability situation.

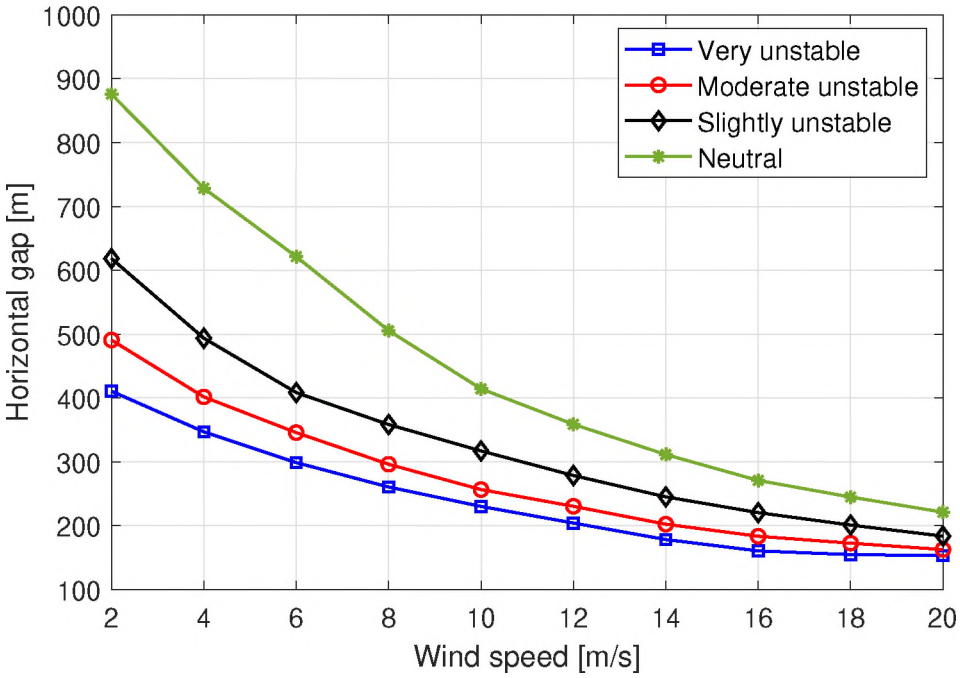

Figure 4.6. The horizontal gap as a function of wind speed for different stability situations.

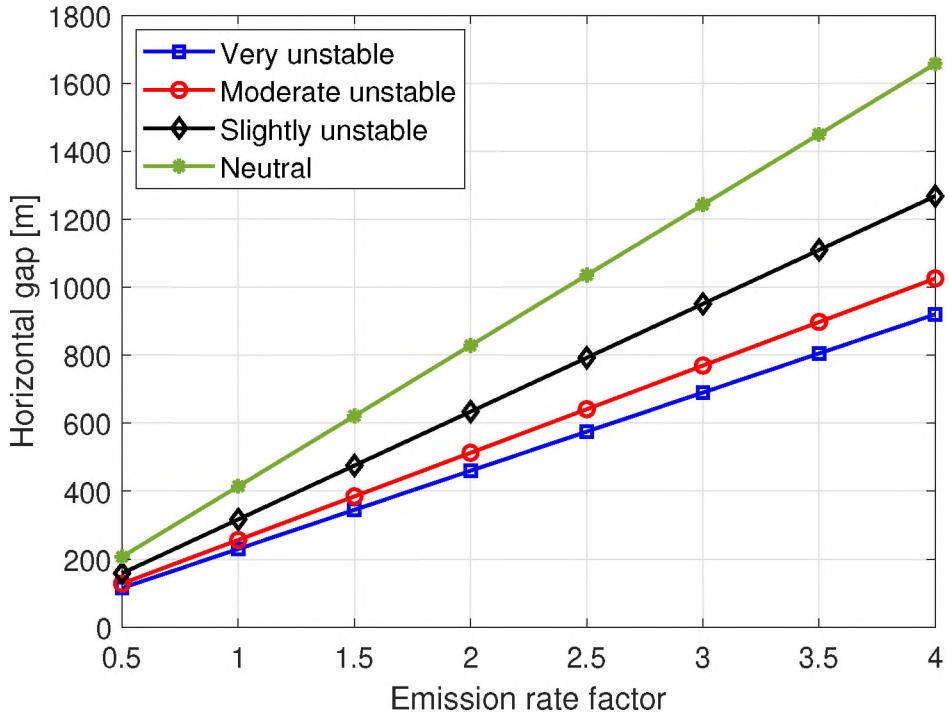

Figure 4.7. The horizontal gap versus emission rate factor for different stability situations.

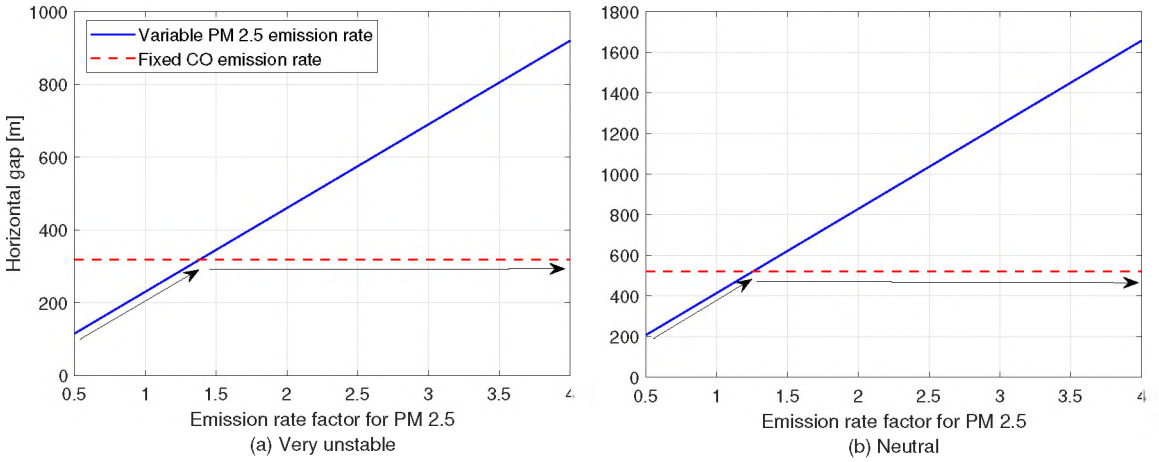

Figure 4.8. The effect of PM2.5 emission rate on the horizontal gap while fixing the emission rate of CO.

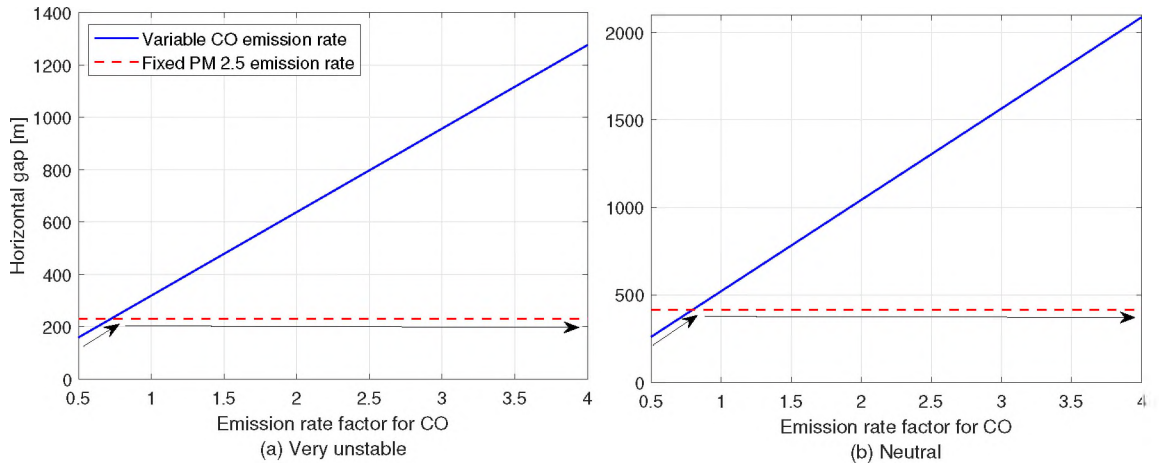

Figure 4.9. The effect of CO emission rate on the horizontal gap while fixing the emission rate of PM2.5.

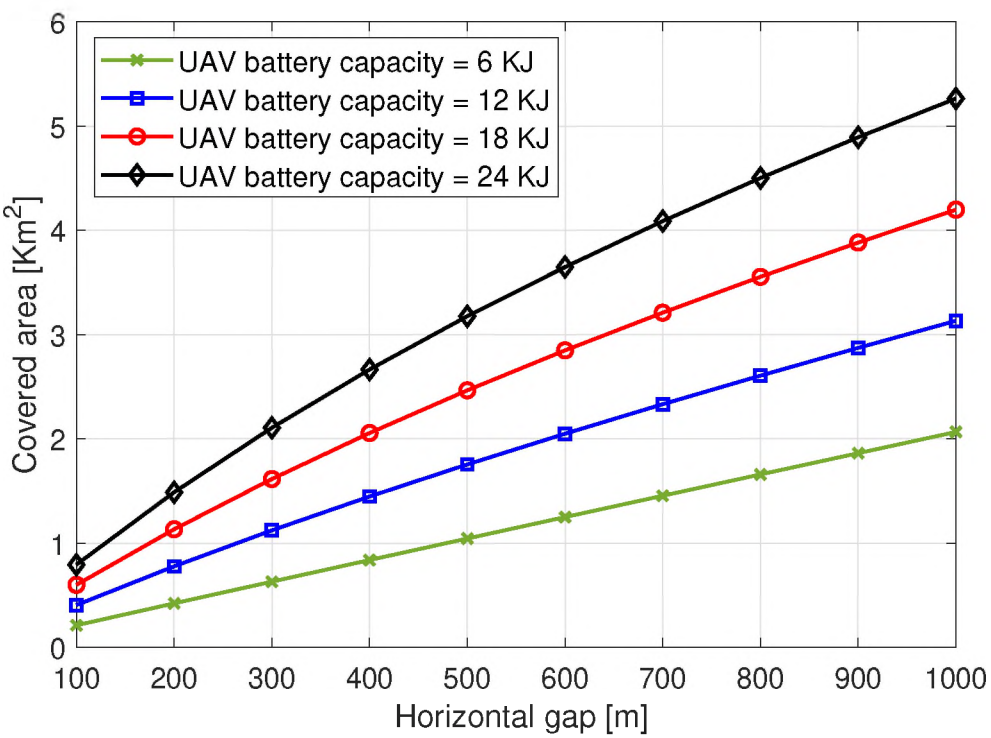

Figure 4.10. The area covered by the UAV as a function of horizontal gap for different UAV battery limitations.

5. COMMUNICATIONS SOLUTION

In this section, the solution to the UAV communication sub-problem was provided. This section optimized communication resources and tried to achieve the desired data rate QoS for each of data type. The communication resources included the UAV transmit power and communication link association between the UAV and BSs. In addition, this section proposed a software design management protocol that managed the resource allocation between the UAV and the selected BS. Finally, the section illustrated simulation results to validate the feasibility of the communication problem solution.

5.1. UAV-BS PROTOCOL

In the proposed protocol, the UAV implemented a software management protocol that managed the transmit power allocation, UAV to BS associations, and UAV's trajectory. Note that a control link was needed between the BSs and UAV. Therefore, establishing a UAV-BS link was required (i.e., this part is booked only for protocol management). In this study, a brief description of a simple management protocol that manages the link between the BS and UAV was given.

5.1.1. Establishment of the UAV-BS Link. To start a communication link between the selected BS and UAV, each BS periodically broadcast a UAVSEARCH frame. The UAV received the UAVSEARCH frame from nearby BSs and checked the pollutants' concentration. The UAV added all BSs to the candidate BSs list. If the pollutants concentration fall below a certain threshold C_{th}, then the UAV ignored these frames, otherwise (i.e., for both pollutants $C[t] \geq C_{th}$) the UAV returned an UAVACK frame to all candidate BSs list containing the UAV's Ethernet/MAC addresses. Note that in the case of multiple UAVs (which can be an extension of this model), it is possible for the BSs to receive multiple UAVACK frames from different UAVs. If this happens, then, a collision protocol must be considered to to avoid the collisions of different UAVACKs arriving to the BSs simultane-

ously. It was assumed that all BSs were connected through optical fibers via a central unit, therefore when the BSs received the UAVACK frame, the central unit selected the best BS to communicate with the UAV. Then, the selected BS responded to the UAV and managed the transmit power allocations for each data type, thus informing the UAV with the best transmit power to send the data over specific bandwidth resources.

5.1.2. Maintenance of the UAV-BS Link. When the communication link between the selected BS and the UAV was established, the UAV was added into "UAV table" of that BS. The table was updated periodically by sending UAVSEARCH-UAVACK messages, as described in the establishment of the UAV-BS link.

5.1.3. Termination of the UAV-BS Link. When the UAV did not respond with an UAVACK to the BS, for certain issues (such as out of range or the concentration of the pollutants are less than the threshold), the BS will update its "UAV table". This update removed the UAV from the table. There were several ways to terminate: 1) graceful leave, where the UAV informed the BS in advance of the termination using CLOSE frame. This could be due to several factors, such as the UAV's battery was down or the concentration of the pollutants were less than the threshold; 2) ungraceful leave, where the UAV terminated the link without informing the BS. In this case, the BS continued tp send UAVSEARCH frames with timeout strategy. This means that the communication link would be terminated when the maximum number of UAVSEARCH frames is reached without responding. Note that the maximum number of UAVSEARCH frames could be selected based on the situation/application.

5.2. COMMUNICATION OPTIMIZATION SOLUTION

In this section, the data transmission optimization problem was formulated to satisfy the QoS constraint given in (3.5) when a wildfire was detected. However, in practice this can be a hard constraint to satisfy $R_{th,n}$ for all time slots due to the limited transmit power circuit or to the randomness of the communication channel gain over time. To avoid the

infeasibility of the problem (i.e., failing achieve the required QoS with the available transmit power budget), the study introduced a fraction variable called loss-factor given by σ to relax $R_{th,n}$, as follows:

$$B_0 \log 2 \left(1 + \frac{P_n[t] g_l[t]}{B_0 N_0}\right) \geq R_{th,n} - \sigma[t] R_{th,n}. \tag{5.1}$$

where $\sigma[t]$ $(0 \leq \sigma[t] \leq 1)$ represents the loss tolerance or loss factor in the rate during time slot t. For example, if $\sigma[t] = 0.2$, the achievable data rate will be lowered by a factor of 0.2. Also, when $\sigma[t] = 0$, $R_{th,n}$ can be achieved. Therefore, the goal was to achieve as close to $R_{th,n}$ as possible by minimizing $\sigma[t]$. The following optimization problem was formulated instantaneously (i.e., for each time slot t), as follows:

$$\underset{\rho_i[t], P_n[t], \epsilon_l[t], \sigma[t]}{\text{minimize}} \quad \sigma[t] \tag{5.2}$$

subject to

$$\rho[t] = \prod_{i=1}^{2} \rho_i[t], \tag{5.3}$$

$$\rho[t] \epsilon_l[t] \left(B_0 \log 2 \left(1 + \frac{P_n[t] g_l[t]}{B_0 N_0}\right) - \left(R_{th,n} - \sigma[t] R_{th,n}\right)\right) \geq 0, \quad \forall n, \forall l, \tag{5.4}$$

$$\sum_{n=1}^{N} P_n[t] \leq \bar{P}, \tag{5.5}$$

$$\sum_{l=1}^{L} \epsilon_l[t] \leq 1, \tag{5.6}$$

$$\sigma[t] \leq 1, \tag{5.7}$$

where constraint (5.7) guarantees that the loss tolerance cannot exceed 1.

5.3. DATA TRANSMISSION OPTIMIZATION SOLUTION

The problem formulated in (5.2)-(5.7) was a mixed integer non-linear optimization problem caused by existence of binary variables $\rho_i[t]$ and $\epsilon_l[t]$ [47]. To simplify the formulated optimization problem, it was solved it in three steps: first, $\rho_i[t]$ was found by comparing the concentration of each pollutant species with the threshold value. Second, the best channel gain was selected between the UAV and BSs, as given in UAV-BS protocol section. Last, given $\rho_i[t]$ and $\epsilon_l[t]$ values, the problem became a convex optimization problem for $P_n[t]$ and $\sigma[t]$ and then the optimal transmit power ($P_n[t]$) and loss tolerance $\sigma[t]$ solution were found by exploiting the strong duality [47]. Therefore, for given given $\rho_i[t]$ and $\epsilon_l[t]$ values, the communication optimization problem formulated in (5.2)-(5.7) becomes:

$$\underset{P_n[t],\sigma[t]\geq 0}{\text{minimize}} \quad \sigma[t] \tag{5.8}$$

subject to

$$\rho[t]\epsilon_l[t]\left(B_0\log_2\left(1+\frac{P_n[t]g_l[t]}{B_0N_0}\right)-\left(R_{th,n}-\sigma[t]R_{th,n}\right)\right)\geq 0, \quad \forall n, \tag{5.9}$$

$$\sum_{n=1}^{N} P_n[t] \leq \bar{P}, \tag{5.10}$$

$$\sigma[t] \leq 1. \tag{5.11}$$

Note that the optimization problem formulated in (5.8)-(5.11) is a convex optimization problem because of: 1) the domain is convex, 2) the objective function is linear (i.e., convex), and 3) all inequality constraints are convex functions. To find optimal transmit power, the study used the Lagrangian method [47]. The Lagrangian expression of (5.8)-(5.11) is derived as:

$$\mathcal{L}(\lambda_{1,n}, \lambda_2, \lambda_3, P_n[t], \sigma[t]) =$$
$$\sigma[t] + \sum_{n=1}^{N} \lambda_{1,n}\rho[t]\epsilon_l[t]\left(\left(R_{th,n} - \sigma[t]R_{th,n}\right) - B_0 \log_2\left(1 + \frac{P_n[t]g_l[t]}{B_0 N_0}\right)\right) \tag{5.12}$$
$$+\lambda_2\left(\sum_{n=1}^{N} P_n[t] - \bar{P}\right) + \lambda_3\left(\sigma[t] - 1\right).$$

In (5.12), $\boldsymbol{\lambda}$ is the vector that contains all the Lagrangian multipliers of the system, where $\lambda_{1,n}$, λ_2, and λ_2 represent the Lagrangian multipliers related to the QoS for data n, peak power, and loss tolerance constraints, respectively. By taking the derivative of the Lagrangian given in 5.12 with respect to $P_n[t]$, and $\sigma[t]$, the optimal transmit power and optimal as follows:

$$P_n[t] = B_0\left(\frac{\lambda_{1,n}\rho[t]\epsilon_l[t]}{\lambda_2 \ln(2)} - \frac{N_0}{g_l[t]}\right)^+, \quad n = 1, .., N. \tag{5.13}$$

$$1 + \lambda_3 = \lambda_{1,n}\rho[t]\epsilon_l[t]R_{th,n}, \quad n = 1, .., N. \tag{5.14}$$

Note that the subgradient method, ellipsoid method, or other heuristic approaches can be employed to find the optimal Lagrangian multipliers of this problem [52].

5.4. COMMUNICATIONS SIMULATION RESULTS

This section presented simulation results to illustrate the communication solution. It was assumed $n = 3$ with different $R_{th,n}$ as $R_{th,1} = 1$[Mbits/s] (for low QoS data rate), $R_{th,2} = 5$[Mbits/s] (for medium QoS data rate), $R_{th,3} = 10$[Mbits/s] (for hight QoS data rate).

The data communication performance is shown in Figure 5.1 and Figure 5.2. Figure 5.1 plots the average achievable data rate for three data rate requirement types: 1) type 1 is suitable for low data rate requirement such as sensor readings, 2) type 2 is suitable medium data rate requirement such as pictures or thermal images, and 3) type 3 is suitable high data rate requirements such as high resolution pictures or acceptable videos quality. Note that, as shown in (5.9), the communications data rate depends on the UAV's transmit

power and loss tolerance. Figure 5.1 showed that the achievable throughput improved with the increase of the power budget $\bar{P}$ up to a certain point. This is due to the fact that starting from this value of $\bar{P}$ the communication data rate threshold was achieved and had no need to consume more energy. Figure 5.1 also showed that when the transmit power budget $\bar{P}$ was low, then the $R_{th,n}$ may not be reached. This could be due to shadowing effect, PL, or communication channel conditions. However, when $\bar{P}$ is high (e.g., 40 dBm W), the loss is zero, and $R_{th,n}$ can be achieved.

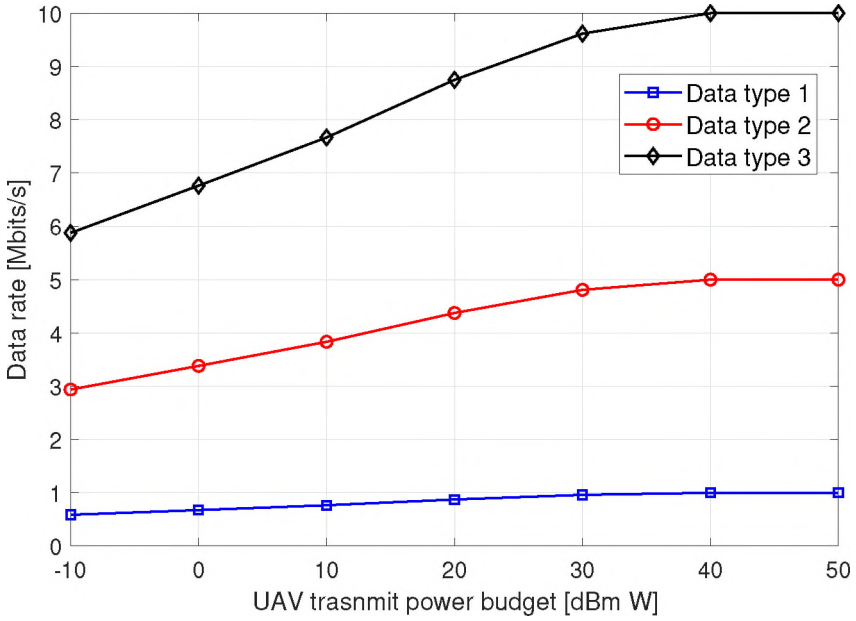

Figure 5.1. Average achievable data rate versus UAV transmit power budget.

By contrast, Figure 5.2 plots the average loss tolerance as a function of the power budget $\bar{P}$. It shown the amount of loss in the target rate threshold versus the UAV power budget $\bar{P}$. For example, if $\bar{P}$ = 10dBm W (i.e., equivalent to 0.01 W), then the average loss in the rate is approximately $0.23R_{th,n}$ for each of the data type n.

Table 5.1, exemplifies the loss tolerance σ, data rate R_n, and transmit power P_n for all three data types and different power budgets $\bar{P}$. This table validates the analysis of when $\bar{P}$ is low, then the optimization problem optimizes the transmit power, thus aiming

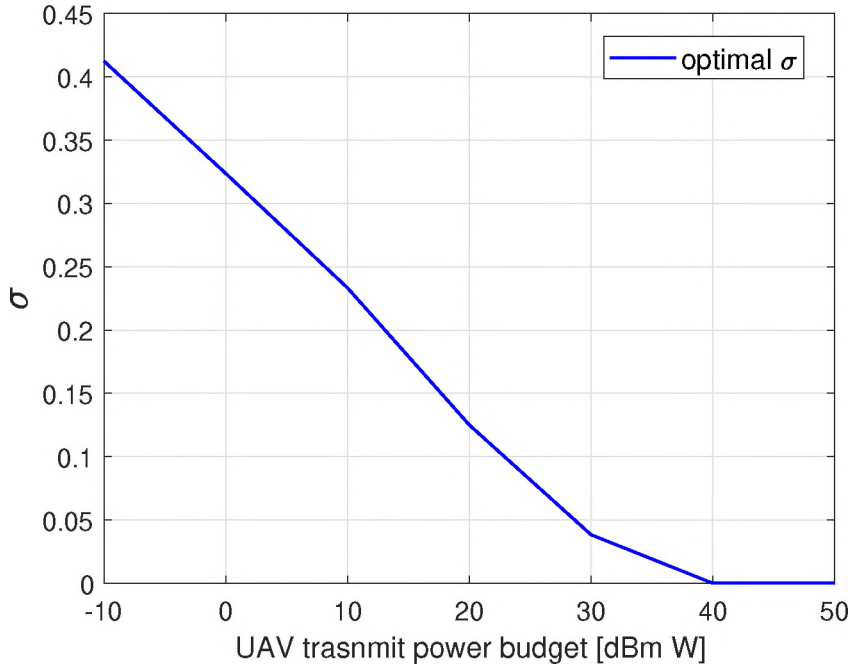

Figure 5.2. Average loss tolerance versus UAV transmit power budget.

Table 5.1. Power allocations and loss-factors based on different UAV's power budget.

	$\bar{P} = 0.1$ W			$\bar{P} = 1$ W		
Data Type	σ	R_n [Mbits/s]	P_n [W]	σ	R_n [Mbits/s]	P_n [W]
1	0.125	0.87	0.016	0.038	0.96	0.29
2	0.125	4.38	0.019	0.038	4.80	0.31
3	0.125	8.75	0.065	0.038	9.62	0.40

to minimize the loss tolerance σ. For example, for data type 2, by using $\bar{P} = 1$W instead of $\bar{P} = 0.1$W, the optimal σ can be decreased from 0.125 to 0.038 and the data rate R_2 increased from 4.38Mbits/s to 4.8Mbits/s.

6. CONCLUSION AND FUTURE DIRECTIONS

This section provided the work conclusion and future directions. This section started by summarizing the work and then exploring two future suggestions.

6.1. CONCLUSION

This study proposed a novel idea for equipping the UAV with air quality sensors and communication transceivers for early wildfire detection. This proposed model can overcome thermal imaging and other current technologies by detecting pollutants faster, and by giving more information about pollutant size distribution. Furthermore, the development of the autonomous patrol optimization (i,e, optimizing the flight track of the UAV) can effectively detect the wildfire events, while preserving the UAV battery for a larger coverage area. This will lead to more robust and energy saving solution for wildfire detection.

6.2. FUTURE DIRECTIONS

The future and ongoing works around this work will implement new research directions to improve the work and lead to better performance.

6.2.1. Multiple Wildfire Hotspot Locations. One future recommendation is to consider multiple wildfire hotspot locations. These location can be determined based on historical data, and it is worth requiring the UAV to patrol above these hotspot locations in a spiral motion. This will come in expense of UAV energy consumption and complexity of the modified track. Figure 6.1 shows the integration between the rectangular track with spiral motion around hotspot locations.

Consider 3D coordinates for each hotspot location j as $\hat{J}_j = (X_j, Y_j, Z_j)$, which is the equivalent altitude over the hotspot location j. Assume that the UAV is initially in the landing location $\hat{L}$ and it will land at the same location after finishing the investigation. For

the path planning problem, at each time slot t, the UAV can be in one of three modes: 1) flying between two hotspots locations (called flying mode), 2) flying around a hotspot location (called hotspot mode), or 3) landing at the initial location (called landing mode). Therefore, the it is needed to introduce three binary variables to identify each mode. Denoting $\tilde{f}[t]$ as flying mode variable and is equal one if UAV is flying between hotspots locations and zero otherwise. Denoting $\tilde{h}_j[t]$ as the hotspot mode variable and is equal to one if the UAV flying over the hotspot j and zero otherwise. Denoting $\tilde{l}[t]$ as the landing mode variable and is equal to one if the UAV is not flying and staying on the landing spot or at the initial location and zero otherwise.

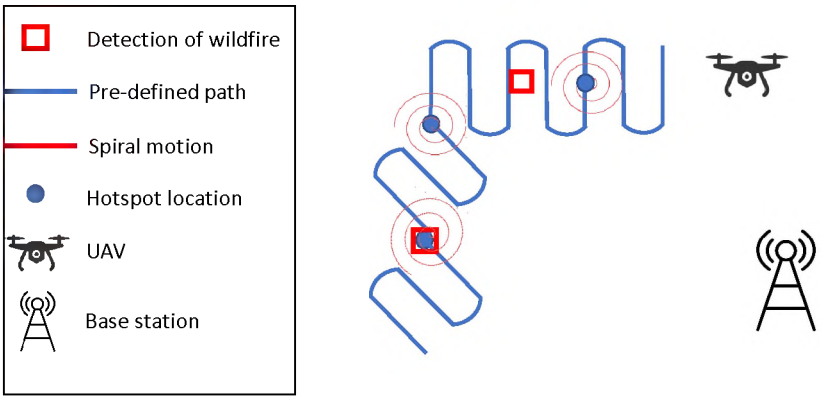

Figure 6.1. Rectangular track with spiral motion around hotspot locations.

The details of these three variables are given as follows:

$$\tilde{f}[t] = \begin{cases} 1, & \text{if the UAV flying between hotspots locations during time slot } t \\ 0, & \text{otherwise.} \end{cases} \tag{6.1}$$

$$\tilde{h}_j[t] = \begin{cases} 1, & \text{if the UAV flying over the hotspot } j \text{ during time slot } t \\ 0, & \text{otherwise.} \end{cases} \tag{6.2}$$

$$\tilde{l}[t] = \begin{cases} 1, \text{ if the UAV not flying and at initial location during time slot } t \\ 0, \text{ otherwise.} \end{cases} \tag{6.3}$$

The following constraints are to ensure the UAV is in one mode only for each time slot t, and to ensure the UAV must fly over all hotspots locations $j = 1, 2, .., J$ within the duration of a total of T time slots:

(to ensure that the UAV is in one mode (either flying or hotspot, or landing).

$$\tilde{f}[t] + \tilde{l}[t] + \sum_{j=1}^{J} \tilde{h}_j[t] = 1, \forall t. \tag{6.4}$$

(to ensure that the UAV flies over all hotspot locations $j = 1, ..., J$).

$$\sum_{t=1}^{T} \tilde{h}_j[t] = 1, \forall j. \tag{6.5}$$

(to ensure that when the UAV is flying over hotspot j, then the coordinate of hotspot j and the coordinate of the UAV are the same).

$$\sum_{t=1}^{T} \tilde{h}_j[t]\hat{U}[t] = \hat{J}_j, \forall j \tag{6.6}$$

(to ensure that when the UAV is landing at the initial location, then the coordinate of initial location and the coordinate of the UAV are the same).

$$\sum_{t=1}^{T} \tilde{l}[t]\hat{U}[t] = \hat{L}. \tag{6.7}$$

Conversely, to perform spiral motion, as shown in Figure 6.2, design parameters must be optimized such as D' (the outer diameter), d' (the inner diameter), and R' (the number of the spiral rings). The values of D', d', and R' can be added to the optimization problem.

The approximated circumference C' of the spiral motion, which is equivalent to the travel path of the UAV when the UAV is flying over a hotspot location and is given as follows:

$$C' = \pi R' \frac{D' + d'}{2}. \tag{6.8}$$

In (6.8), the spiral circumference is approximated by taking the averages of the inner radius and outer radius.

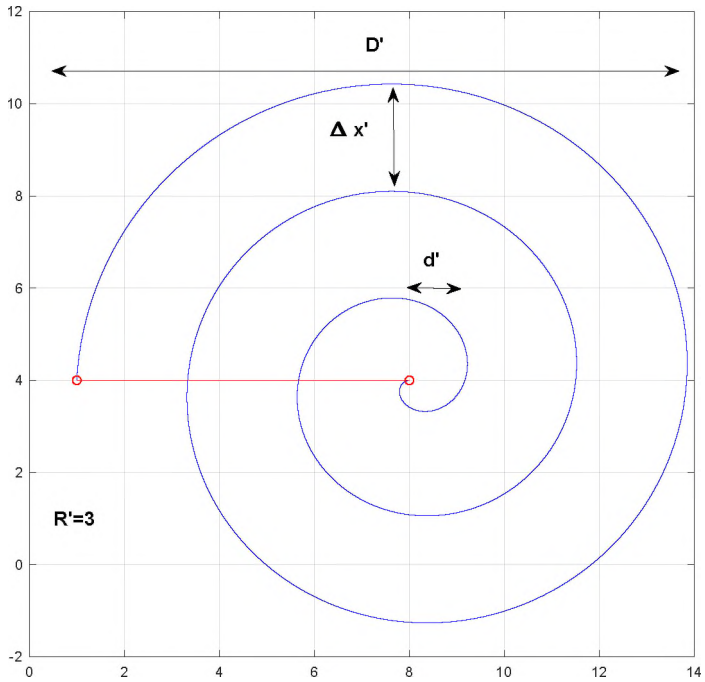

Figure 6.2. An example of spiral motion around a hotspot location centered at (8,4).

6.2.2. Data Transmission via FSO. BSs are not always around or near the forest, therefore it may require long distance communication link. The directional transceiver antennas operating in Terahertz bands, such as free-space-optical (FSO), can provide infrastructure-less wireless access [53]. FSO has recently attracted significant interest from telecommunication researchers and industries, mainly due to the low cost and the

deficit in radio frequency wireless spectrum [54]. FSO uses the unlicensed optical spectrum to provide a higher bandwidth channel for transferring large volumes of data, and it can be easily integrated with the UAV system for transmitting the air quality data collected from the patrol of UAVs [55].

Using a FSO link, the achievable data rate between the UAV and the central unit is a strong function of the geometric loss, as determined by $\bar{r}$ (the radius of the receiver's aperture in m), $\bar{l}$ (the distance between the laser transmitter and receiver in km), and $\bar{\theta}$ (the transmitter divergence angle) as shown in Figure 6.3.

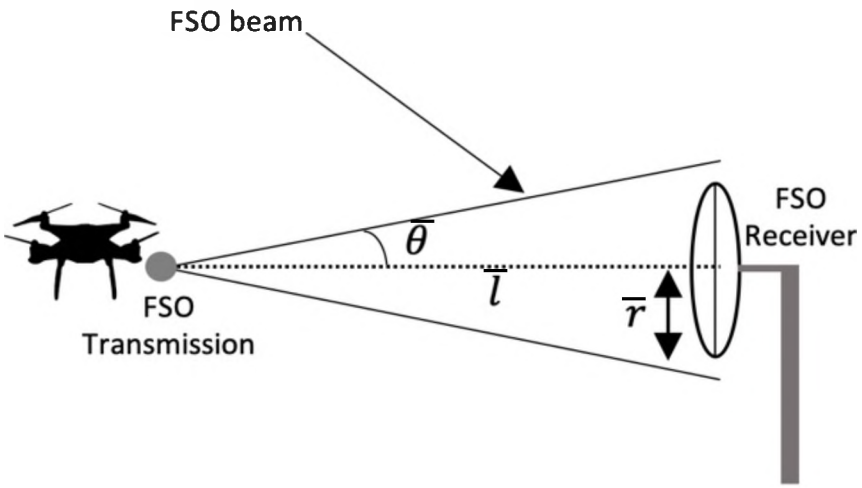

Figure 6.3. FSO transmission model.

FSO in future studies must address research questions related to: 1) optimizing the FSO alignment between the FSO transmitter and receiver. In this case, it is proposed that the UAV can be equipped with a swift and electronic FSO transmitter, 2) optimizing when and where to transmit the collected data to the BS based on weather conditions. For example, the UAV can keep collecting the sensors data and wait until flying over an area

with a clear line-of-sight to transmit the signals to the BS via FSO link, and 3) optimizing the data communication frequency of the UAV, so it does not interfere the UAV flight and air quality sensing.

REFERENCES

[1] D. Kolaric, K. Skala, and A. Dubravic, "Integrated system for forest fire early detection and management," *Periodicum Biologorum*, vol. 110, pp. 205–211, 2008.

[2] Center for Climate and Energy Solutions, "Record wildfires push 2018 disaster costs to $91 billion," 2019. Available [online]: https://www.c2es.org/2019/02/record-wildfires-push-2018-disaster-costs-to-91-billion.

[3] US Today, "Two dead near Los Angeles as Saddleridge fire forces 100,000 people to evacuate," accessed 2021. Available [online]: https://www.usatoday.com/story/news/nation/2019/10/11/california-saddleridge-fire-spreading-evacuations-power-outages/3941274002/.

[4] F. Rego and F. Catry, "Modeling the effects of distance on the probability of fire detection from look outs," *International Journal of Wildland Fire*, vol. 15, pp. 197–202, 2006.

[5] Wikipedia, "Fire lookout tower," accessed 2021. Available [online]: https://en.wikipedia.org/wiki/Firelookouttower.

[6] S. Matthews, A. Sullivan, and J. Gould, "Field evaluation of two image-based wildland fire detection systems," *Fire Safety Journal*, vol. 47, pp. 54–61, 2012.

[7] A. Murray, "Optimising the spatial location of urban fire stations," *Fire Safety Journal*, vol. 62, pp. 64–71, 2013.

[8] S. Bao, N. Xiao, Z. Lai, H. Zhang, and C. Kim, "Optimizing watchtower locations for forest fire monitoring using location models," *Fire Safety Journal*, vol. 71, pp. 100–109, January 2015.

[9] NASA, "Techniques for wildfire detection and monitoring," accessed 2020. Available [online]: https://appliedsciences.nasa.gov/join-mission/training/english/techniques-wildfire-detection-and-monitoring.

[10] Environment and Natural Resources, "Detecting wildfire," accessed 2021. Available [online]: https://www.enr.gov.nt.ca/en/services/wildfire-operations/detecting-wildfire.

[11] NASA, "Techniques for wildfire detection and monitoring," accessed 2021. Available [online]: https://appliedsciences.nasa.gov/join-mission/training/english/techniques-wildfire-detection-and-monitoring.

[12] Z. Gao, L. Zhang, X. Li, M. Liao, and J. Qiu, "Detection and analysis of urban land use changes through multi-temporal impervious," *Journal of Remote Sensing*, vol. 14, pp. 593–606, 2010.

[13] United States Geological Survey (USGS), "Very high-resolution thermal infrared image, fire line temperature in in Tallahassee, FL in 2000," accessed 2021. Available [online]: https://www.usgs.gov/media/images/very-high-resolution-thermal-infrared-image-fire-line-temperature.

[14] ALERTWildfire, "ALERTWildfire project," accessed 2021. Available [online]: http://www.alertwildfire.org/.

[15] J. Pardo, W. Aguilar, and T. Toulkeridis, "Wireless communication system for the transmission of thermal images from a UAV," in *Proc. of Conference on Electrical, Electronics Engineering, Information and Communication Technologies (CHILECON), Pucon, Chile*, pp. 1–5, October 2017.

[16] Y. Wang, J. Li, H. Jing, Q. Zhang, J. Jiang, and P. Biswas, "Laboratory evaluation of three low-cost particle sensors for particulate matter measurement," in *Proc. of the 34th Annual conference American Associations of Aerosol Research, Minneapolis, Minnesota*, October 2015.

[17] Adafruit, "PM2.5 air quality sensor with breadboard adapter," accessed 2021. Available [online]: https://learn.adafruit.com/pm25-air-quality-sensor.

[18] J. Li, H. Li, Y. Ma, Y. Wang, A. Abokifa, C. Lu, and P. Biswas, "Spatiotemporal distribution of indoor particulate matter concentration with a low-cost sensor network," *Building and Environment*, vol. 127, pp. 138–147, January 2018.

[19] Y. Pang, S. Chen, J. An, K. Wang, Y. Deng, A. Benard, N. Lajnef, and C. Cao, "Multilayered cylindrical triboelectric nanogenerator to harvest kinetic energy of tree branches for monitoring environment condition and forest fire," *Advanced Functional Materials*, vol. 30. no. 32, pp. 207–2016, June 2020.

[20] D. Kinaneva, G. V. Hristov, J. Raychev, and P. Zahariev, "Early forest fire detection using drones and artificial intelligence," in *Proc. of the 42nd International Convention on Information and Communication Technology, Electronics and Microelectronics (MIPRO), Opatija Croatia*, pp. 1060–1065, May 2019.

[21] L. Zhang, B. Wang, W. Peng, C. Li, Z. Lu, and Y. Guo, "A method for forest fire detection using UAV," vol. 81, pp. 69–74, 2015.

[22] A. Alsharoa and M. Yuksel, "UAV-Direct: Facilitating D2D communications for dynamic and infrastructure-less networking," in *in Proc. of the 4th ACM Workshop on Micro Aerial Vehicle Networks, Systems, and Applications, Mobile Systems, Applications, and Services (MobiSys), Munich, Germany*, June 2018.

[23] M. Y. Selim, A. Alsharoa, and A. E. Kamal, "Short-term and long-term cell outage compensation using UAVs in 5G networks," in *Proc. of the IEEE Global Communications Conference (GLOBECOM), Abu Dhabi, United Arab Emirates*, pp. 1–6, Dec. 2018.

[24] Incident Information System, "Unmanned aircraft systems use on wildfires," Miller Fire Wildfire news, 2019. Available [online]: https://inciweb.nwcg.gov/incident/article/6417/49578/.

[25] C. Yuan, Z. Liu, and Y. Zhang, "Aerial images-based forest fire detection for firefighting using optical remote sensing techniques and unmanned aerial vehicles," *Journal of Intelligent and Robotic Systems*, vol. 88, p. 635–654, January 2017.

[26] R. S. Allison, J. M. Johnston, G. Craig, and S. Jennings, "Airborne optical and thermal remote sensing for wildfire detection and monitoring," *Sensors*, vol. 16, no. 8, June 2016.

[27] C. Yuan, Z. Liu, and Y. Zhang, "Fire detection using infrared images for UAV-based forest fire surveillance," in *Proc. of the International Conference on Unmanned Aircraft Systems (ICUAS), Miami, FL, USA*, pp. 567–572, June 2017.

[28] South Coast AQMD, "Air quality sensor performance evaluation center," accessed 2020. Available [online]: http://www.aqmd.gov/aq-spec/sensors.

[29] Cooper C. David and F.C. Alley, *Air pollution control : A design approach*. Waveland Press Inc., September 2010.

[30] D. T. Gottuk, M. J. Peatross, R. J. Roby, and C. L. Beyler, "Advanced fire detection using multi-signature alarm algorithms," *Fire Safety Journal*, vol. 37, no. 4, pp. 381 – 394, 2002.

[31] X. Wang, H. Zhou, W. P. Arnott, M. E. Meyer, S. Taylor, H. Firouzkouhi, H. Moosmüller, J. C. Chow, and J. G. Watson, "Evaluation of gas and particle sensors for detecting spacecraft-relevant fire emissions," *Fire Safety Journal*, vol. 113, p. 102977, 2020.

[32] D. Gutmacher, U. Hoefer, and J. Wöllenstein, "Gas sensor technologies for fire detection," *Sensors and Actuators B: Chemical*, vol. 175, pp. 40–45, 2012.

[33] A. Mehadi, H. Moosmüller, D. Campbell, W. Ham, D. Schweizer, L. Tarnay, and J. Hunter, "Laboratory and field evaluation of real-time and near real-time pm2.5 smoke monitors," *Journal of Air Waste Management Associations*, vol. 70, no. 2, p. 158–179, 2019.

[34] S. Illingworth, G. Allen, C. Percival, P. Hollingsworth, M. Gallagher, H. Ricketts, H. Hayes, P. Ładosz, D. Crawley, and G. Roberts, "Measurement of boundary layer ozone concentrations on-board a skywalker unmanned aerial vehicle," *Atmospheric Science Letters*, vol. 15, no. 4, pp. 252–258, March 2014.

[35] Steve Rhode, "Drone search-and-rescue study reveals potential, limits," Aircraft Owners and Pilots Association, October 2018. Available [online]: https://www.aopa.org/news-and-media/all-news/2018/october/01/drone-study-reveals-potential-and-limits.

[36] F. Reisen, C. Meyer, C. Weston, and L. Volkova, "Ground-based field measurements of pm2.5 emission factors from flaming and smoldering combustion in eucalypt forests," *Journal of Geophysical Research: Atmospheres,*, vol. 123, no. 15, pp. 8301–8314, Aug. 2018.

[37] A. Al-Hourani, S. Kandeepan, and A. Jamalipour, "Modeling air-to-ground path loss for low altitude platforms in urban environments," in *Proc. of the IEEE Global Communications Conference (GLOBECOM), Austin, TX, USA*, pp. 2898–2904, Dec. 2014.

[38] A. Hourani, K. Sithamparanathan, and S. Lardner, "Optimal LAP altitude for maximum coverage," *IEEE Wireless Communication Letters*, vol. 3, pp. 569–572, Dec. 2014.

[39] J. Holis and P. Pechac, "Elevation dependent shadowing model for mobile communications via high altitude platforms in built-up areas," *IEEE Transactions on Antennas and Propagation*, vol. 56, pp. 1078–1084, Apr. 2008.

[40] S. L. Cotton, "Human body shadowing in cellular device-to-device communications: Channel modeling using the shadowed $\kappa - \mu$ fading model," *IEEE Journal on Selected Areas in Communications*, vol. 33, no. 1, pp. 111–119, 2015.

[41] S. Obayashi and J. Zander, "A body-shadowing model for indoor radio communication environments," *IEEE Transactions on Antennas and Propagation*, vol. 46, no. 6, pp. 920–927, 1998.

[42] Y. Zheng, Y. Wang, and F. Meng, "Modeling and simulation of pathloss and fading for air-ground link of HAPs within a network simulator," in *Proc. of the IEEE International Conference on Cyber-enabled distributed computing and knowledge discovery (CyberC), Beijing, China*, Oct. 2013.

[43] Y. Zeng and R. Zhang, "Energy-efficient UAV communication with trajectory optimization," *IEEE Transactions on Wireless Communications*, vol. 16, pp. 3747–3760, June 2017.

[44] D. Hulens, J. Verbeke, and T. Goedemé, "Choosing the best embedded processing platform for on-board UAV image processing," in *Proc. of the International joint conference on computer vision, imaging and computer graphics*, pp. 455–472, Springer, 2015.

[45] X. Liu, X. Yu, and Z. Zhang, "PM2.5 concentration differences between various forest types and its correlation with forest structure," *Atmosphere*, vol. 6, no. 11, pp. 1801–1815, 2015.

[46] A. Charland and C. Clements, "Kinematic structure of a wildland fire plume observed by Doppler LiDAR," *IEEE/ACM Transactions on Networking*, vol. 118, no. 8, pp. 3200–3212, 2013.

[47] S. Boyd and L. Vandenberghe, *Convex Optimization*. New York, United States: Cambridge University Press, 2004.

[48] M. Mitchell, *An Introduction to Genetic Algorithms*. Cambridge, MA, USA: MIT Press, 1998.

[49] D. Beasley, D. R. Bull, and R. R. Martin, "An Overview of Genetic Algorithms: Part 2, Research Topics," *University Computing*, vol. 15, no. 4, pp. 170–181, 1993.

[50] B. Wotton, J. Gould, L. McCaw, P. Cheney, and S. Taylor, "Flame temperature and residence time of fires in dry eucalypt forest," *International Journal of Wildland*, vol. 22, no. 3, pp. 270–281, Jan. 2012.

[51] A. Alsharoa, H. Ghazzai, A. Kadri, and A. E. Kamal, "Spatial and temporal management of cellular hetnets with multiple solar powered drones," *IEEE Transactions on Mobile Computing*, vol. 19, no. 4, pp. 954–968, 2020.

[52] S. Boyd and A. Mutapcic, "Stochastic Subgradient Methods." *Notes for EE364, Stanford University*, Winter 2006-07.

[53] A. Sahin, Y. S. Eroglu, I. Guvenc, N. Pala, and M. Yuksel, "Accuracy of AOA-based and RSS-based 3D localization for visible light communications," in *Proc. of the 82nd IEEE Vehicular Technology Conference (VTC-Fall), Boston, MA, USA*, pp. 1–5, 2015.

[54] A. Sevincer, A. Bhattarai, M. Bilgi, M. Yuksel, and N. Pala, "LIGHTNETs: Smart LIGHTing and mobile optical wireless NETworks — A survey," *IEEE Communications Surveys Tutorials*, vol. 15, no. 4, pp. 1620–1641, 2013.

[55] S. Singh, R. Mudumbai, and U. Madhow, "Interference analysis for highly directional 60-GHz mesh networks: The case for rethinking medium access control," *IEEE/ACM Transactions on Networking*, vol. 19, no. 5, pp. 1513–1527, 2011.

VITA

Doaa Rjoub was born in Irbid, Jordan in March 13, 1990. She received the Bachelor of Science degree in Civil Engineering from Al-Balqa Applied University, Jordan, in May 2014. She received the Master of Science degree in Civil Engineering from Missouri University of Science and Technology, U.S.A, in July 2021.

She was the recipient of the Ahel Al Himmeh scholarship in 2009, with full tuition waiver for the Bachelor degree for outstanding students. Her research interests included: air quality sensors, nanoparticle and aerosol instrumentation, unmanned aerial vehicles, water treatment, and water hazard control.